

Variational inference via Gaussian interacting particles in the Bures–Wasserstein geometry

Giacomo Borghi^{*}[†] José A. Carrillo[‡]

January 5, 2026

Abstract

Motivated by variational inference methods, we propose a zeroth-order algorithm for solving optimization problems in the space of Gaussian probability measures. The algorithm is based on an interacting system of Gaussian particles that stochastically explore the search space and self-organize around global minima via a consensus-based optimization (CBO) mechanism. Its construction relies on the Linearized Bures–Wasserstein (LBW) space, a novel parametrization of Gaussian measures we introduce for efficient computations. LBW is inspired by linearized optimal transport and preserves key geometric features while enabling computational tractability. We establish well-posedness and study the convergence properties of the particle dynamics via a mean-field approximation. Numerical experiments on variational inference tasks demonstrate the algorithm’s robustness and superior performance with respect to gradient-based method in presence of non log-concave targets.

Keywords: Gaussian variational inference, Consensus-based optimization, Bures–Wasserstein space, Linear optimal transport, Interacting particle systems

MSC codes: 65C35, 90C26, 49Q22, 60H30, 62F15

1 Introduction

Given a target probability measure $\mu^{\text{targ}} \in \mathcal{P}(\mathbb{R}^d)$ a widespread problem in statistics and computational sciences consists of finding

$$\mu^* \in \operatorname{argmin}_{\mu \in \Pi} \mathcal{D}(\mu \mid \mu^{\text{targ}}) \quad (1.1)$$

where Π is a family of parametrized probability measures, and $\mathcal{D}(\cdot \mid \mu^{\text{targ}})$ is a functional which quantifies the discrepancy from the target. A classical example is the Bayesian inference problem where $\mu^{\text{targ}}(dx) \propto \exp(-V(x))dx$ for some $V : \mathbb{R}^d \rightarrow \mathbb{R}$, and the discrepancy measure corresponds to the Kullback–Leibler divergence, $\mathcal{D}(\cdot \mid \mu^{\text{targ}}) = \text{KL}(\cdot \mid \mu^{\text{targ}})$ [8]. The settings we considered though, are the more general one of Variational Inference (VI), where \mathcal{D} can be given, for instance, by the Maximum Mean Discrepancy, f -divergencies,

^{*}corresponding author

[†]Maxwell Institute for Mathematical Sciences and Department of Mathematics, School of Mathematical and Computer Sciences (MACS), Heriot-Watt University, Edinburgh, UK g.borghi@hw.ac.uk

[‡]Mathematical Institute, University of Oxford, Oxford OX2 6GG, UK jose.carrillo@maths.ox.ac.uk

χ^2 -divergence, Rényi's α -divergence [8, 34]. A regularization term may also be added to make the method more robust.

As for the family of parametrized probability measure, we consider the Gaussian VI problem [22, 30] where $\Pi \subset \mathcal{P}(\mathbb{R}^d)$ is the set of d -dimensional normal distributions

$$\Pi = \mathcal{N}^d := \left\{ \mu = \mathcal{N}(m, \Sigma) \mid m \in \mathbb{R}^d, \Sigma \in \text{Sym}_d^+ \right\}$$

with Sym_d^+ being the space of symmetric positive semi-definite matrices. This approach offers a computationally efficient alternative to traditional Bayesian inference by approximating high-dimensional posterior distributions with tractable Gaussian families, enabling faster approximate inference compared to Markov Chain Monte Carlo methods. While we cannot expect Gaussian distributions to well-approximate an arbitrary multi-modal target, recent theoretical advances provide rigorous error bounds and approximation guarantees, making Gaussian VI particularly appealing in large-scale settings [30, 54].

As explicit solutions are typically not available, one has to rely on optimization algorithms to find a minimizer μ^* to (1.1). While this can be done by applying Euclidean optimization methods at the level of the parameters, better strategies can be developed by exploiting the structure of the space of probability measures where the problem is naturally defined.

Different works, see, for instance, [2, 22, 36], propose first-order algorithms as suitable discretization of gradient flows in the space probability measures [3] equipped with the L^2 -Wasserstein distance. When restricting to the space of non-degenerate Gaussians, the distance is known as the Bures–Wasserstein (BW) distance and can be derived from a suitable Riemannian structure [5, 39]. Gradient descent algorithms with respect to the Hellinger–Kantorovich metric have been recently proposed in [37]. Such optimization dynamics can be conveniently written as a system of ODEs for the mean $m \in \mathbb{R}^d$ and the covariance matrix $\Sigma \in \text{Sym}_d^+$ and have shown superior performance with respect to other Gaussian Bayesian inference methods such as the Laplace method [58], see for instance [36]. As in Euclidean optimization, though, convexity of objective functional plays a central role in deriving convergence guarantees of such gradient-based methods, and the optimizing dynamics may get stuck in local minima, if present.

1.1 Contributions

We consider the more general problem of minimizing an energy functional $\mathcal{E} : \mathcal{P}(\mathbb{R}^d) \rightarrow \mathbb{R}$ over the space of Gaussian measures

$$\mu^* \in \operatorname{argmin}_{\mu \in \mathcal{N}^d} \mathcal{E}(\mu) \tag{1.2}$$

where \mathcal{E} might have several local minima. As we mentioned, gradient-based algorithms are local methods which can fail to find a global minimizers, and several runs with different random initializations might be required to find a suitable solution.

In Euclidean optimization, stochastic particle methods such as Particle Swarm Optimization [31], Genetic Algorithms [29], Simulated Annealing [33], and Consensus-Based Optimization (CBO) [47], offers a viable alternative to solve global optimization problems. These gradient-free methods are typically based on a system of interacting particles which stochastically explore the search space and eventually self-organize around a solution to (1.2). They have been empirically shown to be efficient, robust against local minima, and they can be theoretically studied under the lenses of statistical physics, see e.g. the review [11] and the references therein.

In this work, we propose a CBO-type dynamics which exploits the Bures–Wasserstein geometry of \mathcal{N}^d to solve (1.2). In the Euclidean CBO algorithm, each particle stochastically

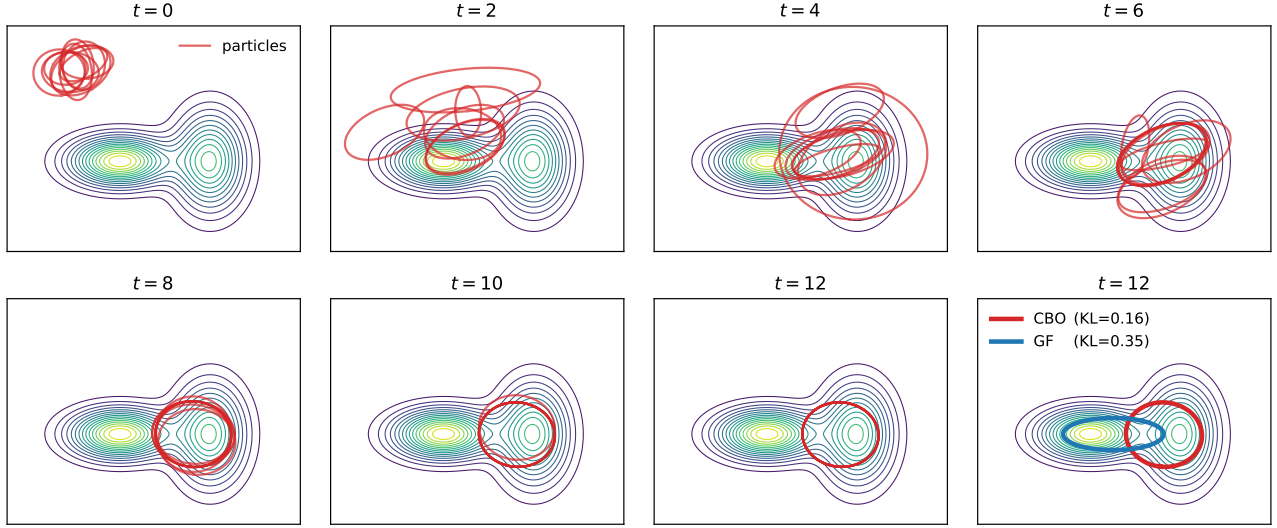


Figure 1: Evolution of $N = 10$ Gaussian particles for minimization of $\mathcal{E} = \text{KL}$ divergence from target bi-modal measure (contour lines). Particles evolve according to the CBO-type dynamics we design in this paper for problems of type (1.2) (see Section 4 for the definition). Final plot compares the solution computed by the CBO algorithm with the one of BW Gradient Flow algorithm [36]. Corresponding KL values are also shown. Supplementary videos illustrating the evolution are available here [9].

moves towards a consensus point consisting of a weighted average of the entire ensemble. Higher weights are given to particles attaining low objective value so that the consensus point can be considered a proxy for the minimizer. Our starting point is the deterministic particle system studied in [12] where each particle is a probability measure and the Euclidean average is substituted with the metric Wasserstein barycenter [1]. In our Gaussian settings, every particle is a Gaussian measure

$$\mu_t^i = \mathcal{N}(m_t^i, \Sigma_t^i), \quad \text{for } i = 1, \dots, N, \quad t \geq 0$$

and, thanks to the fact that the L^2 -Wasserstein barycenter is still a Gaussian, the consensus-dynamics of [12] reads

$$\begin{cases} (\bar{m}_t, \bar{\Sigma}_t) := \text{Barycenter}^\omega \{ (m_t^i, \Sigma_t^i) \mid i = 1, \dots, N \} \\ \frac{d}{dt} m_t^i = \bar{m}_t - m_t^i & i = 1, \dots, N \\ \frac{d}{dt} \Sigma_t^i = \bar{\Sigma}_t (\Sigma_t^i \bar{\Sigma}_t)^{-\frac{1}{2}} - I & i = 1, \dots, N. \end{cases} \quad (1.3)$$

Above, the barycenter serves as the consensus point and is computed according to the weight function

$$\omega(\mu) := \exp(-\alpha \mathcal{E}(\mu)) \quad \alpha \gg 1, \quad (1.4)$$

and the tangent vector $\bar{\Sigma}_t (\Sigma_t^i \bar{\Sigma}_t)^{-\frac{1}{2}} - I$ corresponds the optimal transport maps from Σ_t^i to $\bar{\Sigma}_t$, see Section 2 for more details on the definition of the barycenter and the BW geometry. A part from [12], consensus dynamics in Wasserstein spaces have been formulated in [6, 7, 19] with aim of deriving a distributed algorithm for the computation of Wasserstein barycenters, and not in the context of optimization.

While coherent with the BW geometry, the particle system (1.3) lacks stochasticity and is computationally expensive to implement, making it unsuitable for solving the optimization problem (1.2). To address this, the contributions of this work are:

- i) We propose the Linearized Bures–Wasserstein space (LBW), a novel parametrization of the space of Gaussian measures that enables efficient computation and the use of stochastic analysis, while retaining key features of the BW geometry. This is inspired by Linearized Optimal Transport [35, 40], where probability measures are represented via optimal transport maps from a fixed reference measure;
- ii) We design an efficient CBO-type dynamics in the LBW space to solve problems of the form (1.2). The particle method is gradient-free and only requires evaluations of the objective functional \mathcal{E} (up to a constant). We study the well-posedness of the system and its convergence towards minimizers via a mean-field approximation of the dynamics;
- iii) We validate the algorithm on various Gaussian VI test problems and investigate the role of different parameters. Comparisons with gradient-based methods demonstrate the superior performance of Gaussian CBO in non-convex settings.

The novelty of our contributions extends beyond the specific CBO algorithm we propose. Indeed, we demonstrate that the computational paradigm of particle systems can be extended beyond Euclidean settings, provided the ambient space has sufficient structure and supports efficient simulation. Also, the LBW parametrization of \mathcal{N}^d shows how to introduce stochasticity into Gaussian VI algorithms in a geometrically meaningful way, potentially enhancing the performance of gradient-based optimizers too.

1.2 Outline

In Section 2 we introduce the notation and recall the BW Riemannian geometry. Sections 3 and 4 include the main contributions of the paper: the novel LBW parametrization of \mathcal{N}^d and the Gaussian CBO particle system which we also theoretically analyze. In Section 5 we numerically validate the algorithm against different VI test problems. We conclude the paper with an outlook on future research perspectives in Section 6.

2 Notation and preliminaries

The set $\mathcal{P}(\mathbb{R}^d)$ is the set of Borel probability measure over \mathbb{R}^d , and $\mathcal{P}_2(\mathbb{R}^d)$ is the subset of measures with bounded second moments: $\mu \in \mathcal{P}(\mathbb{R}^d)$ with $M_2(\mu) := (\int |x|^2 \mu(dx))^{1/2} < \infty$. $\mathcal{P}_2^{ac} \subset \mathcal{P}(\mathbb{R}^d)$ is the subset of measures admitting a density with respect to Lebesgue and we will sometimes abuse the notation by denoting the density of μ with $\mu = \mu(x)$ itself. For a point $x \in \mathbb{R}^d$, $\delta_x \in \mathcal{P}(\mathbb{R}^d)$ is the Dirac measure: $\delta_x(A) = 1$ if $x \in A$, and 0 otherwise.

With Sym_d we indicate the set of $d \times d$ symmetric matrices, while $\text{Sym}_d^+, \text{Sym}_d^{++} \subset \text{Sym}_d$ are, respectively, the sets of positive semi-definite and positive definite symmetric matrices. Given a mean $m \in \mathbb{R}^d$ and a covariance matrix Sym_d^+ , we indicate the correspondent Gaussian probability measure with $\mathcal{N}(m, \Sigma)$, and with $\mathcal{N}^d \subset \mathcal{P}_2(\mathbb{R}^d)$ the set of all Gaussian probability measures over \mathbb{R}^d . For any $A, B \in \text{Sym}_d$ we write $A \succeq B$ if $A - B \in \text{Sym}_d^+$ and $A \succ B$ if $A - B \in \text{Sym}_d^{++}$. The trace operator is given by $A \in \mathbb{R}^{d \times d}$, $\text{tr}(A) = \sum_{i=1}^d A_{ii}$, and for $A \in \text{Sym}_d^{++}$, $\sqrt{A} = B$ where B is the unique matrix $B \in \text{Sym}_d^{++}$ such that $BB = A$.

Random variables are assumed to be defined on a common probability space $(\Omega, \mathcal{F}, \mathbb{P})$. We write $X \sim \mu$, if X is a random variable with law $\mu \in \mathcal{P}(\mathbb{R}^d)$. For two $\mu, \nu \in \mathcal{P}_2(\mathbb{R}^d)$ the L^2 -Wasserstein distance [51] is defined as

$$\mathbb{W}(\mu, \nu) := \sqrt{\inf_{X \sim \mu, Y \sim \nu} \mathbb{E}|X - Y|^2}.$$

Given two Gaussians $\mu = \mathcal{N}(m, \Sigma)$ and $\nu = \mathcal{N}(\bar{m}, \bar{\Sigma})$ which are non-singular, that is, $\Sigma, \bar{\Sigma} \in \text{Sym}_d^{++}$, the L^2 -Wasserstein distance takes the explicit form [23, 27, 41]

$$\mathbb{W}(\mu, \nu) = \sqrt{|m - \bar{m}|^2 + \text{tr}(\Sigma) + \text{tr}(\bar{\Sigma}) - 2\text{tr}(\Sigma^{1/2}\bar{\Sigma}\Sigma^{1/2})^{1/2}}.$$

With a slight abuse of notation, for two zero-mean Gaussian measures we will sometimes use the shorter $\mathbb{W}(\Sigma, \bar{\Sigma})$ to indicate $\mathbb{W}(\mathcal{N}(0, \Sigma), \mathcal{N}(0, \bar{\Sigma}))$. In the literature, this is referred to as the Bures–Wasserstein distance, as it also coincides with the Bures metric [59] between covariance matrices in quantum information theory.

Let $\omega : \mathcal{P}(\mathbb{R}^d) \rightarrow [0, +\infty)$ be a weight function. Given a collection of probability measures $\mu^1, \dots, \mu^N \in \mathcal{P}_2(\mathbb{R}^d)$, the weighted Wasserstein barycenters, or Fréchet means, are defined as the solutions to the problem

$$\bar{\mu} \in \underset{\nu \in \mathcal{P}_2(\mathbb{R}^d)}{\operatorname{argmin}} \sum_{i=1}^N \omega(\mu^i) \mathbb{W}^2(\mu^i, \bar{\mu}). \quad (2.1)$$

The notion of barycenter generalizes the notion of mean to metric spaces, and uniqueness in the Wasserstein space is ensured only in presence of probability densities, see [1] for more details. Moreover, if the measures are non-singular Gaussians, $\mu^i = \mathcal{N}(m^i, \Sigma^i)$, $i = 1, \dots, N$, the barycenter is unique and it is also a Gaussian $\bar{\mu} = \mathcal{N}(\bar{m}, \bar{\Sigma})$ with mean and covariance matrix characterized by the equations

$$\bar{m} = \sum_{i=1}^N \frac{\omega(\mu^i)}{\sum_j \omega(\mu^j)} m^i, \quad \bar{\Sigma} = \sum_{i=1}^N \frac{\omega(\mu^i)}{\sum_j \omega(\mu^j)} \left((\Sigma^i)^{1/2} \bar{\Sigma} (\Sigma^i)^{1/2} \right)^{1/2}. \quad (2.2)$$

We note that the barycenter mean takes an explicit form, while the covariance matrix is the solution of a matrix equation, which is well-defined [50]. The equation can be used for the computation of the barycenter via a fixed point iteration [62] which is proven to converge with a rate [18]. This strategy corresponds to solving (2.1) through a (Wasserstein) gradient descent algorithm with step size 1, see [61].

2.1 Bures–Wasserstein manifold

The convenience of working with Gaussian measures goes beyond having explicit formulas for \mathbb{W} and simpler characterization of barycenters. The space of non-singular Gaussians with the L^2 -Wasserstein metric attains the much richer structure of a Riemannian manifold, known as the Bures–Wasserstein (BW) manifold [5, 39, 56].

We identify the space of non-singular Gaussian measure with $\mathbb{R}^d \times \text{Sym}_d^{++}$. At every point $(m, \Sigma) \in \mathbb{R}^d \times \text{Sym}_d^{++}$, the tangent space is given by $T_{(m, \Sigma)}(\mathbb{R}^d \times \text{Sym}_d^{++}) = \mathbb{R}^d \times T_{\Sigma} \text{Sym}_d^{++}$ with

$$T_{\Sigma} \text{Sym}_d^{++} = \text{Sym}_d.$$

In the literature, one can find two different parametrizations of the BW Riemannian metric on $T_{\Sigma} \text{Sym}_d^{++}$: one introduced in [56], and the other one studied in [5, 39]. We use the former as it consistent with the classical Riemannian-like structure of the L^2 -Wasserstein space introduced in the seminal paper by F. Otto for the porous medium equation [42]. Moreover, it allows for more efficient computations of exponential maps, see Remark 2.2 for a comparison with the alternative parametrization presented in [5, 39]. For any $T, S \in T_{\Sigma} \text{Sym}_d^{++}$, the Riemannian metric is given by

$$d_{\Sigma}(T, S) = \text{tr}(T \Sigma S) =: \langle T, S \rangle_{\Sigma}. \quad (2.3)$$

The Riemannian exponential map is defined by

$$\exp_{\Sigma}(T) := (I + T) \Sigma (I + T) \quad \text{for } T \succ -I. \quad (2.4)$$

The condition $T \succ -I$ is required to ensure that $(I + T)\Sigma(I + T) \succ 0$, that is, $\exp_{\Sigma}(T) \in \text{Sym}_d^{++}$. Therefore, the BW manifold is not geodesically complete and the definition domain of the exponential is the translated open cone $\text{Sym}_d^{++} - I$. The Riemannian logarithm between $\Sigma, \bar{\Sigma} \in \text{Sym}_d^{++}$ is given by

$$\log_{\Sigma}(\bar{\Sigma}) := \bar{\Sigma}(\Sigma\bar{\Sigma})^{-\frac{1}{2}} - I, \quad (2.5)$$

and corresponds to the optimal transport map (shifted by I) between $\mathcal{N}(0, \Sigma)$ and $\mathcal{N}(0, \bar{\Sigma})$, that is,

$$\mathbb{W}^2(\Sigma, \bar{\Sigma}) = \mathbb{E}|X - (I + \log_{\Sigma}(\bar{\Sigma}))X|^2 \quad \text{with } X \sim \mathcal{N}(0, \Sigma).$$

The restriction $T \succ -I$ on the exponential map T becomes now intuitive in light of Brenier's theorem [13]: as the optimal transport map needs to be the gradient of a convex function, we have indeed that $x^T(I + T)x$ is convex only provided $I + T \succeq 0$. The case where $I + T$ is only positive semi-definite is excluded as it would transport $\mathcal{N}(0, \Sigma)$ to a singular Gaussian, thus leaving the BW manifold. More generally, we underline that the BW geometry is coherent with the formal Otto Riemannian geometry [42], which is actually rigorous when restricting to the space of probabilities with smooth positive densities [38].

Furthermore, the space of Gaussian measures can be seen as a stratified space of manifolds, each corresponding to a different rank of the covariance matrix [57]. While Wasserstein distance between singular Gaussians are well-defined, the Riemannian structure is lost at the boundary of the BW manifold. We note that this stratified structure of sub-manifolds appears also in the larger L^2 -Wasserstein space, see [49, Remark 2.1].

Remark 2.1. *The BW geometry is only one of the possible choices of Riemannian geometry for Sym_d^{++} . A popular choice, for instance, is the Affine Invariant (AI) metric [44]. In [28], the authors compare the two metrics concluding that BW is more suitable for optimization in Sym_d^{++} thanks to its non-negative curvature and linear dependence on the space. Also, we note that the exponential maps in the form (2.4) is computationally cheap to evaluate. This is an important feature that will allow us in the next section to parameterized the space Sym_d^{++} via tangent vectors.*

Remark 2.2. *In [5, 39] the authors propose a different definition of the Riemannian metric on $T\text{Sym}_d^{++}$ given by*

$$\tilde{d}_{\Sigma}(V, U) := \frac{1}{2}\text{tr}(\mathcal{L}_{\Sigma}[V]U) \quad (2.6)$$

for $V, U \in \text{Sym}_d$ and $\Sigma \in \text{Sym}_d^{++}$, where $\mathcal{L}_{\Sigma}[V]$ is known as the Lyapunov operator, and it is the unique solution to the Lyapunov equation $\mathcal{L}_{\Sigma}[V]\Sigma + \Sigma\mathcal{L}_{\Sigma}[V] = V$. The corresponding exponential map is studied in details in [57] and it is given by

$$\widetilde{\exp}_{\Sigma}(V) = \Sigma + V + \mathcal{L}_{\Sigma}[V]\Sigma\mathcal{L}_{\Sigma}[V].$$

The relation between the different metrics proposed, (2.3) and (2.6), is given by

$$T = \mathcal{L}_{\Sigma}[V].$$

The literature for the computation of the Lyapunov operator is particularly rich and it includes methods for large-scale matrices too, see the review paper [53]. As mentioned in [28], the cost of exact computation is the same as matrix exponential or inversion, that is, $\mathcal{O}(d^3)$. The exponential map (2.4), instead, requires to perform matrix multiplications.

3 Linearized Bures–Wasserstein space

The Linear Optimal Transport (LOT) distance is a computationally efficient metric between probability measures which has recently gained popularity in applications [14, 35, 40, 52]. Consider a reference probability measure $\mu^0 \in \mathcal{P}_2^{ac}(\mathbb{R}^d)$, and $\mu^1, \mu^2 \in \mathcal{P}_2(\mathbb{R}^d)$. Let $\mathcal{T}_1, \mathcal{T}_2 : \mathbb{R}^d \rightarrow \mathbb{R}^d$ the optimal transport maps from μ^0 to μ^1, μ^2 , respectively. That is, we have that $\mathbb{W}(\mu^0, \mu^1)^2 = \mathbb{E}|X - \mathcal{T}_1(X)|^2$ if $X \sim \mu^0$, and the same holds for μ^2 . The LOT distance with base μ^0 is given by

$$\text{LW}_{\mu^0}(\mu^1, \mu^2) := \mathbb{E}|\mathcal{T}_1(X) - \mathcal{T}_2(X)|^2 \quad \text{for } X \sim \mu^0, \quad (3.1)$$

or, equivalently, it corresponds to the weighted L^2 norm $\|\mathcal{T}_1 - \mathcal{T}_2\|_{L^2(\mu^0)}$ between the OT maps. Derived as a simplified version of the Wasserstein metric, its main feature is that it allows to compute the mutual distances between N probability measures by solving only N optimal transport problems (instead of the N^2 required by \mathbb{W}).

We apply the LOT approach to the BW space to derive the LBW metric between Gaussian measures. As we expect, this corresponds to the BW Riemannian metric at a reference Gaussian measure μ^0 .

To show this, we first recall that if $Y \sim \mathcal{N}(0, \Sigma)$, then $\mathbb{E}|Y|^2 = \text{tr}(\Sigma)$ and, for $A \in \text{Sym}_d$, it holds $AY \in \mathcal{N}(0, A\Sigma A)$. Consider now $\mu^0 = \mathcal{N}(0, \Sigma^0)$, $\Sigma^0 \in \text{Sym}_d^{++}$, and, for simplicity, two other zero-mean measures $\mu^1 = \mathcal{N}(0, \Sigma^1)$, $\mu^1 = \mathcal{N}(0, \Sigma^1)$, $\Sigma^1, \Sigma^2 \in \text{Sym}_d^{++}$. We note that the optimal transport map between zero-mean Gaussians is a linear map, and in particular, from (2.4) and (2.5) it holds $\mathcal{T}_i(x) = (I + \log_{\Sigma^0}(\Sigma^i))x$, $i = 1, 2$. Direct computations show that the LOT distance corresponds to the BW metric at $T_{\Sigma^0}\text{Sym}_d^{++}$:

$$\begin{aligned} \text{LW}_{\mu^0}(\mu^1, \mu^2)^2 &= \mathbb{E}|\mathcal{T}_1(X) - \mathcal{T}_2(X)|^2 \\ &= \mathbb{E}|(\mathcal{T}_1(X) - X) - (\mathcal{T}_2(X) - X)|^2 \\ &= \mathbb{E}|\log_{\Sigma^0}(\Sigma^1) - \log_{\Sigma^0}(\Sigma^2)|^2 \\ &= \text{tr}((\log_{\Sigma^0}(\Sigma^1) - \log_{\Sigma^0}(\Sigma^2)) \Sigma^0 (\log_{\Sigma^0}(\Sigma^1) - \log_{\Sigma^0}(\Sigma^2))) \\ &= \|\log_{\Sigma^0}(\Sigma^1) - \log_{\Sigma^0}(\Sigma^2)\|_{\Sigma^0}^2 \end{aligned}$$

since $\text{tr}(A\Sigma^0 B) = \langle A, B \rangle_{\Sigma^0}$ from (2.3). Of course, if we include arbitrary means $m^1, m^2 \in \mathbb{R}^d$, for $\mu^1 = \mathcal{N}(m^1, \Sigma^1)$, $\mu^2 = \mathcal{N}(m^2, \Sigma^2)$ the same computations lead to

$$\text{LW}_{\mu^0}(\mu^1, \mu^2)^2 = |m^1 - m^2|^2 + \|\log_{\Sigma^0}(\Sigma^1) - \log_{\Sigma^0}(\Sigma^2)\|_{\Sigma^0}^2. \quad (3.2)$$

3.1 Geodesics, barycenters and extension of exponential maps

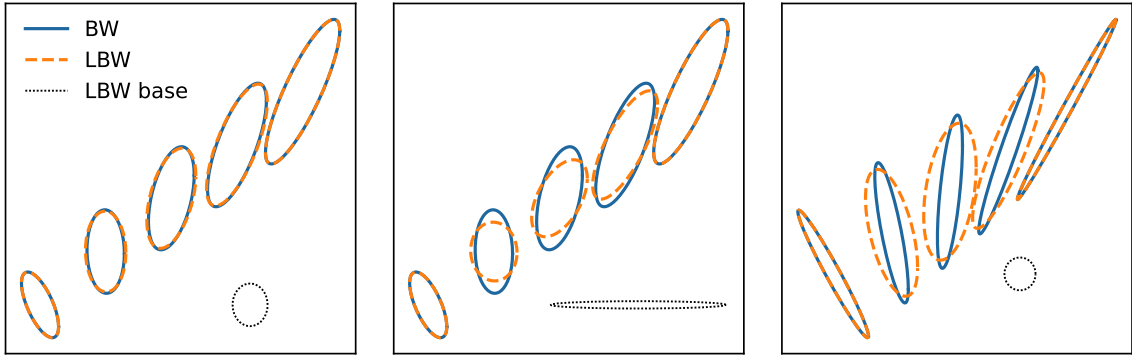
Geodesics in the LBW geometry corresponds to the Wasserstein generalized geodesics [3] and are given by $\mu(\tau) = \mathcal{N}(m(\tau), \Sigma(\tau))$ $\tau \in [0, 1]$ with

$$m(\tau) = (1 - \tau)m^1 + \tau m^2, \quad \Sigma(\tau) = \exp_{\Sigma^0}((1 - \tau)\log_{\Sigma^0}(\Sigma^1) + \tau \log_{\Sigma^0}(\Sigma^2)).$$

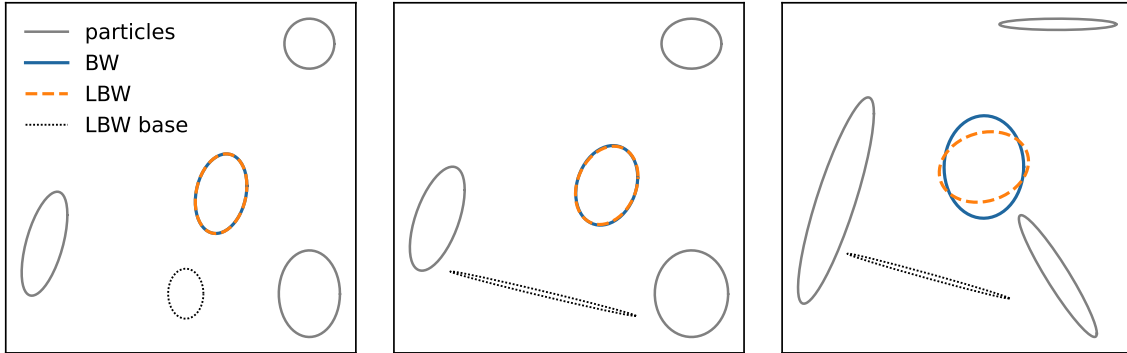
In Figure 2a we compare BW and LBW geodesics for different values of $\Sigma^0, \Sigma^1, \Sigma^2$. The two geometries seem to diverge the more the covariance matrices are close to being singular.

Barycenters in LBW take an explicit form, unlike BW barycenters. Consider N Gaussian particles $\mu^i = \mathcal{N}(m^i, \Sigma^i)$, $i = 1, \dots, N$, their weighted LBW barycenter is directly given by $\bar{\mu} = \mathcal{N}(\bar{\mu}, \bar{\Sigma})$ with

$$\bar{m} = \sum_{i=1}^N \frac{\omega(\mu^i)}{\sum_j \omega(\mu^j)} m^i, \quad \bar{\Sigma} = \exp_{\Sigma^0} \left(\sum_{i=1}^N \frac{\omega(\mu^i)}{\sum_j \omega(\mu^j)} \log_{\Sigma^0}(\Sigma^i) \right). \quad (3.3)$$



(a) Geodesics in the BW and LBW spaces



(b) Barycenters between 3 Gaussian particles in the BW and LBW spaces

Figure 2: Visual comparison between the geometry of BW and its linearization LBW. Different scenarios are considered, and, in particular, different base measures for LBW are used. Each Gaussian measure $\mathcal{N}(m, \Sigma)$ is represented by an ellipsis centered at the mean m and stretched according to the covariance matrix Σ .

Note that if we identify Σ^i with the corresponding tangent vector $T^i = \log_{\Sigma^0}(\Sigma^i)$ the characterization of the barycenter reduces to

$$\bar{T} = \sum_{i=1}^N \frac{\omega(\mu^i)}{\sum_j \omega(\mu^j)} T^i. \quad (3.4)$$

While it may not be obvious by their respective expressions (2.2) and (3.3), the LBW barycenter corresponds to a first order approximation to the BW one. As shown in [61], the LBW barycenter vector \bar{T} corresponds to the (negative) gradient of the BW barycenter functional (2.1). As we can see from Figure 2b, this approximation can be fairly accurate if, again, the Gaussian particles are far from the singularity.

Following the LOT approach, we are identifying each non-degenerate Gaussian measure with its corresponding BW tangent vector. Since the BW manifold is geodesically incomplete and the exponential domain is $\text{Sym}_d^{++} - I$ (not the entire tangent space Sym_d), the parametrization of the covariance matrices is given by

$$\begin{aligned} (\text{Sym}_d^{++} - I) &\rightarrow \text{Sym}_d^{++} \\ T &\mapsto \Sigma = \exp_{\Sigma^0}(T). \end{aligned}$$

To be able to parametrize every Gaussian measure, possibly with a singular covariance matrix, we can extend by continuity the definition domain to the closed convex cone

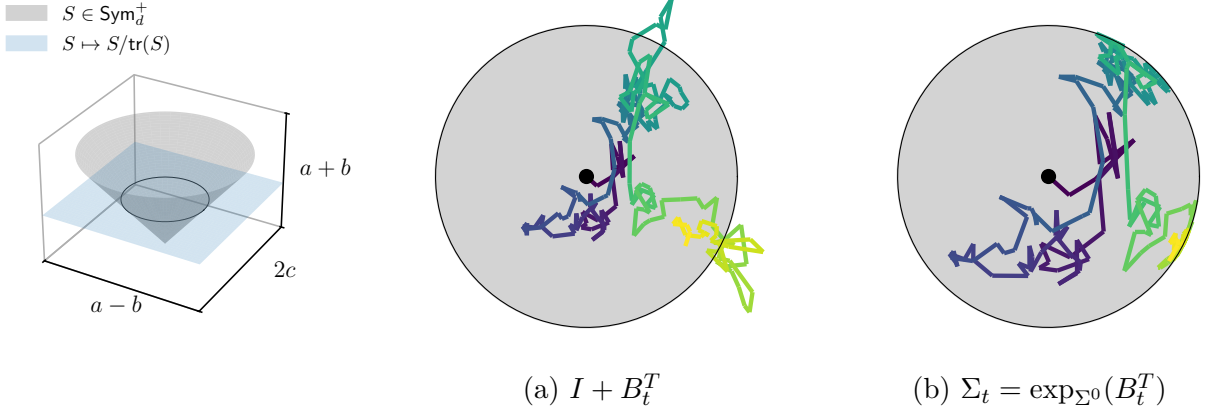


Figure 3: A Brownian path in LBW space. If B_t^T is a Brownian particle in Sym_d , it may leave the cone of optimal transport maps, see (a) (equivalently, $I + B_t^T$ leaves the cone of positive semi-definite matrices Sym_d^+). The extended exponential map (2.4), though, automatically reflects the dynamics so that $\Sigma_t = \exp_{\Sigma^0}(B_t^T) \in \text{Sym}_d^+$ without additional computational effort, see (b). To visualize a symmetric matrix $S = (a, c; c, b)$, we first map it to \mathbb{R}^3 as $(a - b, 2c, a + b)$. The cone Sym_d^+ is then given by $z \geq \sqrt{x^2 + y^2}$. The 2-dimensional plot is finally obtained by projection towards trace 1 matrices $S \mapsto S/\text{tr}(S)$ (or, equivalently, $(x, y, z) \mapsto (x, y)/z$).

$\text{Sym}_d^+ - I$. We will go further and extend its definition to the entire space Sym_d by simply setting

$$\exp_{\Sigma^0}(T) := (I + T)\Sigma^0(I + T) \quad \text{for any } T \in \text{Sym}_d.$$

Note that the exponential always satisfies $\exp_{\Sigma^0}(T) \in \text{Sym}_d^+$.

To sum up, given a base Gaussian measure $\mu^0 = \mathcal{N}(m^0, \Sigma^0)$, $m^0 \in \mathbb{R}^d$, $\Sigma \in \text{Sym}_d^{++}$, the LBW space can be identified as the finite-dimensional Euclidean space

$$\mathbb{R}^d \times \text{Sym}_d \quad \text{with product} \quad \langle m^1, m^2 \rangle + \langle T^1, T^2 \rangle_{\Sigma^0} \quad (3.5)$$

for any $(m^1, T^1), (m^2, T^2) \in \mathbb{R}^d \times \text{Sym}_d$, and we denote with $\|\cdot\|_{\text{LBW}(\Sigma^0)}$ the respective norm. While this leads to a redundant parametrization of \mathcal{N}_d , we obtain the computational benefit of dealing with an unconstrained space rather than the open cone $\text{Sym}_d^{++} - I$. This is particularly convenient for the definition of Brownian Gaussian particles.

3.2 Brownian processes in LBW

We construct a Brownian process in LBW by starting from an orthonormal basis. Note that the dimension of Sym_d is $d(d + 1)/2$ and that, for $\Sigma^0 = I$ an orthogonal basis is simply given by symmetric matrices with either only one non-zero entry at the diagonal, or two non-zero entries off the diagonal. We refer to Section 5 for a discussion on how to generate an orthonormal basis $\{e_\ell\}_{\ell=1}^{d(d+1)/2}$ for an arbitrary $\Sigma^0 \in \text{Sym}_d^{++}$. Consider now a Brownian process $(B_t^m)_{t \geq 0}$ in \mathbb{R}^d and $d(d + 1)/2$ i.i.d. one-dimensional Brownian processes $\{(\xi^\ell)_{t \geq 0}\}_{\ell=1}^{d(d+1)/2}$. We can construct a Brownian process in LBW as

$$B_t := (B_t^m, B_t^T) \quad \text{where} \quad B_t^T := \sum_{\ell=1}^{d(d+1)/2} e_\ell \xi_t^\ell. \quad (3.6)$$

It is interesting to note that the associated probability measure

$$\mu_t = \mathcal{N}(B_t^m, \Sigma_t) \quad \text{with} \quad \Sigma_t = \exp_{\Sigma^0}(B_t^T)$$

is a random process taking values in the space \mathcal{N}_d of Gaussian measures. Moreover, it explores the entire \mathcal{N}_d , including Gaussians with singular covariance matrix, going therefore beyond the BW space. Figure 3 shows a Brownian path B_t^T and the corresponding covariance matrix Σ_t via a 2-dimensional projection of the dynamics.

Remark 3.1. *In principle, one could choose to restrict the LBW space to the closed cone of optimal transport maps, that is, constrain the tangent vector $T \in \text{Sym}_d$ to the closed convex cone $\text{Sym}_d^+ - I$ by including suitable boundary conditions. The random process exploring the space would then consist of a reflected SDE [46] whose numerical simulation requires to project the dynamics back to the cone at every time iteration [45]. Therefore, for computational efficiency, we chose here to simply extend the domain of the map $\exp_{\Sigma^0}(\cdot)$ to the entire space Sym_d , and to consider unconstrained dynamics.*

4 Gaussian consensus-based optimization

4.1 The particle dynamics

We are now ready to define the Consensus-Based Optimization particle system in the linearized Bures–Wasserstein space. The N Gaussian particles at time $t \geq 0$ are described tangent vectors at the reference measures $\mu^0 = \mathcal{N}(0, \Sigma^0), \Sigma^0 \in \text{Sym}_d^{++}$

$$(m_t^i, T_t^i) \in \mathbb{R}^d \times \text{Sym}_d \quad i = 1, \dots, N$$

via the relation

$$\mu_t^i = \mathcal{N}(m_t^i, \Sigma_t^i) \quad \text{with} \quad \Sigma_t = \exp_{\Sigma^0}(T_t^i).$$

Recall the CBO dynamics [47] is characterized by a deterministic component which drives particles towards the consensus point and a stochastic component favoring exploration of the search space.

As in the deterministic consensus dynamics (1.3), the consensus point corresponds to a weighted barycenter, now computed according to the LBW geometry. To stress the the dependence of the barycenter on the entire particle system, we introduce the empirical measure

$$\rho_t^N = \frac{1}{N} \sum_{i=1}^N \delta_{(m_t^i, T_t^i)} \in \mathcal{P}(\mathbb{R}^d \times \text{Sym}_d).$$

The consensus point is then given by the weighted LBW barycenters (3.3), (3.1), with the exponential weights (1.4). For an arbitrary measure $\rho \in \mathcal{P}(\mathbb{R}^d \times \text{Sym}_d)$, it reads

$$\bar{m}^\alpha[\rho] := \frac{\int m e^{-\alpha \mathcal{E}^\#(m, T)} \rho(dm, dT)}{\int e^{-\alpha \mathcal{E}^\#(m, T)} \rho(dm, dT)}, \quad \bar{T}^\alpha[\rho] := \frac{\int T e^{-\alpha \mathcal{E}^\#(m, T)} \rho(dm, dT)}{\int e^{-\alpha \mathcal{E}^\#(m, T)} \rho(dm, dT)} \quad (4.1)$$

where, for notational simplicity, we introduced the finite-dimensional objective function

$$\mathcal{E}^\#(m, T) := \mathcal{E}(\mathcal{N}(m, \exp_{\Sigma^0}(T))).$$

For the empirical measure ρ_t^N , the consensus point $(\bar{m}^\alpha[\rho_t^N], \bar{T}^\alpha[\rho_t^N])$ reduces to a weighted sum of the particles, which, for $\alpha \gg 1$, is close to the best particles among the ensemble thanks to the Boltzmann–Gibbs exponential weights. To be specific, if at time $t \geq 0$ there is a particle attaining a lower objective value with respect to all the others, it holds

$$(\bar{m}^\alpha[\rho_t^N], \bar{T}^\alpha[\rho_t^N]) \longrightarrow \operatorname{argmin}_{(m_t^i, T_t^i), i=1, \dots, N} \mathcal{E}^\#(m_t^i, T_t^i) \quad \text{as} \quad \alpha \rightarrow \infty.$$

Therefore, the consensus point can be considered a proxy for the best particle of the ensemble.

Given two vectors $a, b \in \mathbb{R}^d$, we denote with $a \odot b \in \mathbb{R}^d$ the component-wise product, $(a \odot b)_\ell = a_\ell b_\ell$. We fix a basis $\mathbf{e} = \{e_\ell\}_{\ell=1}^{d(d+1)/2}$ for Sym_d orthonormal with the respect to $\langle \cdot, \cdot \rangle_{\Sigma^0}$. For $S, T \in \text{Sym}_d$, we define the component-wise product as

$$T \odot S := \left(\sum_\ell T_\ell^{\mathbf{e}} e_\ell \right) \odot \left(\sum_\ell S_\ell^{\mathbf{e}} e_\ell \right) = \sum_\ell T_\ell^{\mathbf{e}} S_\ell^{\mathbf{e}} e_\ell$$

which corresponds to the component-wise product between the vectors of coefficients $(T_1^{\mathbf{e}}, \dots, T_{d(d+1)/2}^{\mathbf{e}})$, $(S_1^{\mathbf{e}}, \dots, S_{d(d+1)/2}^{\mathbf{e}})$. Let $B_t^i = (B_t^{i,m}, B_t^{i,T})$ be N independent Brownian processes taking values in $\mathbb{R}^d \times \text{Sym}_d$ constructed with the basis \mathbf{e} (see (3.6)).

The CBO dynamics in LBW space reads

$$\begin{cases} dm_t^i &= \lambda(\bar{m}^\alpha[\rho_t^N] - m_t^i)dt + \sigma(\bar{m}^\alpha[\rho_t^N] - m_t^i) \odot dB_t^{i,m} \\ dT_t^i &= \lambda(\bar{T}^\alpha[\rho_t^N] - T_t^i)dt + \sigma(\bar{T}^\alpha[\rho_t^N] - T_t^i) \odot dB_t^{i,T} \end{cases} \quad i = 1, \dots, N \quad (4.2)$$

supplemented with initial conditions $(m_0^i, T_0^i) \sim \rho_0$, i.i.d, for some $\rho_0 \in \mathcal{P}(\mathbb{R}^d \times \text{Sym}_d)$. Above, $\lambda, \sigma > 0$ are two parameters controlling the strength of the deterministic and stochastic components respectively. We note that noise is possibly degenerate as it depends on the differences $(\bar{m}^\alpha[\rho_t^N] - m_t^i)$ and $(\bar{T}^\alpha[\rho_t^N] - T_t^i)$. In this way, particles which are far from the consensus point tend to have a more explorative behavior than those close to it. This is an essential mechanism for ensuring emergence of consensus as the particles evolve. Also, the diffusion is anisotropic since each direction is explored at a different rate. This strategy has been proposed in [17] for superior performance in high-dimensional problems.

It is important to remark that, thanks to (4.1)-(4.2) and the definition of \odot , the CBO dynamics in LBW corresponds to the standard Euclidean CBO particle system if we identify each T_t^i with its coefficients associated with the basis $\mathbf{e} = \{e_\ell\}_{\ell=1}^{d(d+1)/2}$. Therefore, (4.2) corresponds to a CBO dynamics in \mathbb{R}^D with $D = d + d(d+1)/2$, and we can rely on the standard well-posedness results for CBO particle systems [16, 17]. We recall them in the following for completeness and translate the assumption on the (finite-dimensional) objective function $\mathcal{E}^\# = \mathcal{E}^\#(m, T)$ into assumptions on the functional $\mathcal{E} = \mathcal{E}(\mu)$ for better interpretability.

Lemma 4.1. *Let $\Sigma^0 \in \text{Sym}_d^{++}$ and $\mu^0 = \mathcal{N}(0, \Sigma^0)$. Assume $\mathbb{E}|m_0^i|^2, \mathbb{E}\|T_0^i\|_{\Sigma^0}^2 < 0$, and that, for some $L_\mathcal{E} > 0$ it holds for any $\mu^1, \mu^2 \in \mathcal{P}_2(\mathbb{R}^d)$*

$$|\mathcal{E}(\mu^1) - \mathcal{E}(\mu^2)| \leq L_\mathcal{E} (1 + M_2(\mu^1) + M_2(\mu^2)) \mathbb{W}_{\mu^0}(\mu^1, \mu^2). \quad (4.3)$$

Then, system (4.2) admits a unique strong solution.

Proof. Recall from (3.5) that the LBW norm on $\mathbb{R}^d \times \text{Sym}_d$ with base Σ^0 is given by $\|(m, T)\|_{\text{LBW}(\Sigma^0)}^2 = |m|^2 + \|T\|_{\Sigma^0}^2$. We first notice that the locally Lipschitz continuity assumption on $\mathcal{E}^\#$ is equivalent to show

$$\begin{aligned} |\mathcal{E}^\#(m^1, T^1) - \mathcal{E}^\#(m^2, T^2)| &\leq L_\mathcal{E} (1 + \|(m^1, T^1)\|_{\text{LBW}(\Sigma^0)} + \|(m^2, T^2)\|_{\text{LBW}(\Sigma^0)}) \\ &\quad \times \|(m^1, T^1) - (m^2, T^2)\|_{\text{LBW}(\Sigma^0)}. \end{aligned}$$

This is also an equivalent condition to (4.3) since $M_2(\mu^i)$ and $\|(m^i, T^i)\|_{\text{LBW}(\Sigma^0)}$ are equivalent up to a positive constant:

$$M_2(\mu^i)^2 = |m^i|^2 + \text{Tr}((I + T^i)\Sigma^0(I + T^i)) = |m^i|^2 + \|I + T^i\|_{\Sigma^0}^2, \quad (4.4)$$

and since $\text{LBW}_{\mu^0}(\mu^1, \mu^2) = \|(m^1, T^1) - (m^2, T^2)\|_{\text{LBW}(\Sigma^0)}$. After identifying $\mathbb{R}^d \times \text{Sym}_d$ with \mathbb{R}^D for given an orthonormal basis, we can use the well-posedness result [16, Theorem 2.1] which states that the dynamics is well-posed for a locally Lipschitz, finite-dimensional, objective function $\mathcal{E}^\#$. \square

Let us discuss what type of functional \mathcal{E} satisfy condition (4.3). For energy functionals of type

$$\mathcal{V}(\mu) = \int V(x)\mu(dx), \quad \mathcal{W}(\mu) = \iint W(x, y)\mu(dx)\mu(dy) \quad (4.5)$$

a sufficient condition for (4.3) is the local Lipschitz continuity of V and W . More delicate is the case of the log-entropy (relevant for the KL divergence)

$$\mathcal{U}(\mu) = \begin{cases} \int \log(\mu(x))\mu(dx) & \text{if } \mu \ll \mathcal{L}^d \\ +\infty & \text{otherwise} \end{cases}$$

as it takes the infinite value for singular Gaussian measures. Though, \mathcal{U} satisfies a local Lipschitz bound for the L^2 -Wasserstein distance \mathbb{W} (which is stronger than a bound for LBW_{μ^0}) under a regularity condition:

Proposition 4.1 ([48, Proposition 1]). *Let $\mu^1, \mu^2 \in \mathcal{P}_2^{ac}(\mathbb{R}^d)$, and (c_1, c_2) -regular, that is, such that*

$$|\nabla \log \mu^i(x)| \leq c_1|x| + c_2,$$

then

$$|\mathcal{U}(\mu^1) - \mathcal{U}(\mu^2)| \leq \left(c_2 + \frac{c_1}{2} M_2(\mu^1) + \frac{c_1}{2} M_2(\mu^2) \right) \mathbb{W}(\mu^1, \mu^2). \quad (4.6)$$

For $\mu = \mathcal{N}(m, \Sigma)$ with $\Sigma \succcurlyeq \varepsilon I$, $\varepsilon > 0$, it holds

$$|\nabla \log \mu(x)| = |\Sigma^{-1}(x - m)| \leq \varepsilon^{-1}(|x| + |m|),$$

so the regularity assumption is satisfied uniformly for Gaussians with bounded eigenvalues. Let $\text{clip}_\varepsilon : \text{Sym}_d^+ \rightarrow \{\Sigma \in \text{Sym}_d^{++} : \Sigma \succcurlyeq \varepsilon I\}$ be the function which clips the eigenvalues to a minimum value $\varepsilon > 0$ defined by

$$\Sigma = \sum_{\ell=1}^d \lambda_\ell u_\ell u_\ell^\top \quad \mapsto \quad \text{clip}_\varepsilon(\Sigma) := \sum_{\ell=1}^d (\lambda_\ell \wedge \varepsilon) u_\ell u_\ell^\top$$

where $(\lambda_\ell, u_\ell)_\ell$ is an eigenbasis for Σ as in [36]. We may now regularize the entropy functional by substituting it with

$$\mathcal{U}_\varepsilon(\mu) := \mathcal{U}(\mathcal{N}(m, \text{clip}_\varepsilon(\Sigma))) \quad \text{for } \mu = \mathcal{N}(m, \Sigma). \quad (4.7)$$

This modification does not affect the location of the minimizers for $\varepsilon \ll 1$ and ensures well-posedness of the particle system (4.2). More general internal energies can also be considered provided they satisfy (4.3).

Assuming $\mu^{\text{targ}} \propto \exp(-V)$, we obtained therefore well-posedness of Gaussian CBO dynamics for the regularized KL divergence $\mathcal{E} = \text{KL}_\varepsilon(\cdot | \mu^{\text{targ}}) = \mathcal{V} + \mathcal{U}_\varepsilon$. We remark that the clipping is only necessary for the well-posedness of the time-continuous dynamics, and that, in practice, one can implement the algorithm by simply truncating the value of \mathcal{E} .

Remark 4.1. *An alternative discrepancy measure to the KL divergence is the Maximum Mean Discrepancy (MMD) induced by a reproducing kernel Hilbert space (RKHS). Under suitable smoothness and normalization conditions on the kernel, one can prove that the MMD is controlled by the Wasserstein distance. In particular, as shown in [60, Proposition 2, Corollary 3], it holds*

$$\|\mu^1 - \mu^2\|_{\mathcal{H}_\kappa} \leq C\mathbb{W}(\mu^1, \mu^2),$$

for a constant C depending on the curvature of the kernel at the origin. We refer to [60] and the references therein for more details and the definition of the norm $\|\cdot\|_{\mathcal{H}_\kappa}$ associated to the reproducing kernel space \mathcal{H}_κ .

4.2 Mean-field analysis and convergence towards global minima

Mean-field approximations of interacting particle systems are a powerful tool to study their long time behavior. For CBO methods, the mean-field analysis allows to investigate the effectiveness of the algorithm by studying the convergence of the particles towards global minimizers [16, 17, 24]. We show in this section that the same type of analysis also applies to the Gaussian CBO particle system (4.2). As for Lemma 4.1, we can rely entirely on the results available in the literature for standard CBO in \mathbb{R}^D thanks to the finite-dimensional and Euclidean nature of $\mathbb{R}^d \times \text{Sym}_d$ equipped with the LBW product. We translate, when possible, the assumptions on $\mathcal{E}^\#$ into assumptions on \mathcal{E} .

The mean-field approximation to the particle system (4.2) can be formally derived by assuming propagation of chaos of the particle system [55]. Let $F_t \in \mathcal{P}((\mathbb{R}^d \times \text{Sym}_d)^N)$ be the particles joint probability measure. If $F_0 = \rho_0^{\otimes N}$, we assume that for large particle systems $N \gg 1$ the distribution at $t \geq 0$ can be approximated as

$$F_t \approx \rho_t^{\otimes N} \quad \text{for some } \rho_t \in \mathcal{P}(\mathbb{R}^d \times \text{Sym}_d).$$

This means that the particles are i.i.d also at subsequent times $t \geq 0$, and that each of them evolves according to the McKean–Vlasov process

$$\begin{cases} dm_t &= \lambda(\bar{m}^\alpha[\rho_t] - m_t)dt + \sigma(\bar{m}^\alpha[\rho_t] - m_t) \odot dB_t^m \\ dT_t &= \lambda(\bar{T}^\alpha[\rho_t] - T_t)dt + \sigma(\bar{T}^\alpha[\rho_t] - T_t) \odot dB_t^T \\ \rho_t &= \text{Law}(m_t, T_t). \end{cases} \quad (4.8)$$

Note that the average mean $\bar{m}^\alpha[\rho_t^N]$ is above substituted by $\bar{m}^\alpha[\rho_t]$, which depends on the own law ρ_t of the mean-field particle.

Assumption 4.1. *The objective functional \mathcal{E} is bounded from below over \mathcal{N}^d , $\underline{\mathcal{E}} := \inf_{\mu \in \mathcal{N}^d} \mathcal{E}(\mu)$ and locally Lipschitz continuous (4.3). Furthermore, either \mathcal{E} is bounded from above, $\sup_{\mu \in \mathcal{N}^d} \mathcal{E}(\mu) < \infty$, or it grows quadratically at infinity:*

$$\mathcal{E}(\mu) - \underline{\mathcal{E}} \geq c_l M_2(\mu)^2 \quad \text{for } \mu, M_2(\mu) \geq R,$$

for some constants $R, c_l > 0$.

Lemma 4.2. *Let $\mu^0 = \mathcal{N}(0, \Sigma^0)$, $\Sigma^0 \in \text{Sym}_d^{++}$, \mathcal{E} satisfy Assumption 4.1, and $\rho_0 \in \mathcal{P}_4(\mathbb{R}^d \times \text{Sym}_d)$. Then, there exists a unique non-linear process $(m, T) \in \mathcal{C}([0, \infty), \mathbb{R}^d \times \text{Sym}_d)$ satisfying (4.8) in a strong sense with $\lim_{t \rightarrow 0} \rho_t = \rho_0 \in \mathcal{P}_2(\mathbb{R}^d \times \text{Sym}_d)$.*

Proof. As in Lemma 4.1, well-posedness of the mean-field dynamics follows from well-posedness of the mean-field CBO dynamics in \mathbb{R}^D . In [17] the authors prove well-posedness provided the finite-dimensional objective $\mathcal{E}^\#$ satisfies

- i) $\underline{\mathcal{E}} = \inf \mathcal{E}^\# > -\infty$;
- ii) there exists constants $\tilde{L}_\mathcal{E}, \tilde{c}_u$ such that for all $z_1 = (m^1, T^1), z_2 = (m^2, T^2)$

$$\begin{cases} |\mathcal{E}^\#(z_1) - \mathcal{E}^\#(z_2)| \leq \tilde{L}_\mathcal{E} (1 + \|z_1\|_{\text{LBW}(\Sigma^0)} + \|z_2\|_{\text{LBW}(\Sigma^0)}) \|z_1 - z_2\|_{\text{LBW}(\Sigma^0)} \\ \mathcal{E}^\#(z_1) - \underline{\mathcal{E}} \leq \tilde{c}_u (1 + \|z_1\|_{\text{LBW}(\Sigma^0)}^2), \end{cases}$$

- iii) either $\sup \mathcal{E}^\# < +\infty$ or there exists \tilde{M}, \tilde{c}_l such that for all z

$$\mathcal{E}^\#(z) - \underline{\mathcal{E}} \geq \tilde{c}_l \|z\|_{\text{LBW}(\Sigma^0)}^2 \quad \text{for } \|z\|_{\text{LBW}(\Sigma^0)} \geq \tilde{R},$$

see [17, Assumption 3.1, Theorem 3.1, Theorem 3.2]. Condition i) is equivalent to what we have assumed in Assumption 4.1. We note that condition ii) is a small modification of [17, Assumption 3.1] where the Lipschitz constant takes the form $(\|z_1\| + \|z_2\|)$, but this change does have an impact on the proof. Also, the quadratic upper bound follows from the local Lipschitz assumption. Altogether, thanks to the equivalence between the LBW norm and the second moment $M_2(\mu)$ for the corresponding measure μ (see (4.4)), then condition ii) follows from the locally Lipschitz condition (4.3) on \mathcal{E} . For the same reason, also the quadratic lower bound iii) for $\mathcal{E}^\#$ is equivalent (up to constants) to the quadratic lower bound in Assumption 4.1 for \mathcal{E} . \square

We have already discussed under which conditions the functionals $\mathcal{V}, \mathcal{W}, \mathcal{U}$ satisfy the local Lipschitz continuity (4.3). Lower bound for \mathcal{V}, \mathcal{W} follows from lower bound the V and W respectively. Clearly, if $\inf V, \inf W > -\infty$, then $\inf \mathcal{V}, \inf \mathcal{W} > -\infty$. Also, if V grows quadratically at infinity, so does \mathcal{V} : let

$$V(x) - \inf V \geq 2c_l|x|^2 \quad \text{for } |x| > R,$$

then, for μ such that $M_2(\mu) \geq R/\sqrt{2}$, it holds

$$\begin{aligned} \int V(x)\mu(dx) - \inf V &\geq 2c_l \int_{|x|>R} |x|^2\mu(dx) + \int_{|x|\leq R} (V(x) - \inf V)\mu(dx) \\ &\geq 2c_l \int_{|x|>R} |x|^2\mu(dx) \pm 2c_l \int_{|x|\leq R} |x|^2\mu(dx) \\ &\geq 2c_l \int |x|^2\mu(dx) - 2c_l R^2 \\ &\geq 2c_l M_2(\mu)^2 - c_l M_2(\mu)^2 = c_l M_2(\mu)^2 \end{aligned}$$

where in the second line we used that $V(x) - \inf V \geq 0$.

For \mathcal{W} , let $\inf W > -\infty$ and consider a similar growth condition

$$W(x, y) - \inf W \geq 2c_l(|x|^2 + |y|^2) \quad \text{for } |x|^2 + |y|^2 > R.$$

Note that, differently from \mathcal{V} , in general $\inf \mathcal{W} \neq \inf W$, and $\inf W \leq \inf \mathcal{W}$. Consider

$$M_2(\mu) \geq \max\{R/\sqrt{2}, \Delta \mathcal{W}/c_l\}, \quad \text{where } \Delta \mathcal{W} := \inf W - \inf \mathcal{W} \geq 0.$$

Similar computations as above lead to the following

$$\begin{aligned} \int W(x, y)\mu(dx)\mu(dy) - \inf \mathcal{W} &= \int W(x, y)\mu(dx)\mu(dy) - \inf W - \Delta \mathcal{W} \\ &\geq 2c_l \iint_{|x|^2+|y|^2>R} (|x|^2 + |y|^2)\mu(dx)\mu(dy) \\ &\quad + 2c_l \iint_{|x|^2+|y|^2\leq R} (W(x, y) - \inf W)\mu(dx)\mu(dy) - \Delta \mathcal{W} \\ &\geq 2c_l \iint_{|x|^2+|y|^2>R} (|x|^2 + |y|^2)\mu(dx)\mu(dy) \pm 2c_l \iint_{|x|^2+|y|^2\leq R} (|x|^2 + |y|^2)\mu(dx)\mu(dy) - \Delta \mathcal{W} \\ &\geq 4c_l M_2(\mu)^2 - 4c_l R^2 - \Delta \mathcal{W} \\ &\geq c_l(4 - 2 - 1)M_2(\mu)^2 = c_l M_2(\mu)^2. \end{aligned}$$

For \mathcal{U} , we cannot expect quadratic growth at infinity, nor boundedness. Therefore, only the clipped version \mathcal{U}_ε (4.7) satisfies Assumption 4.1 and, as a consequence, the same holds for the KL_ε divergence from a target $\mu^{\text{targ}} \propto \exp(-V)$.

We note that the formal derivation of the mean-field approximation can be actually substituted, in the case of CBO-type dynamics, by rigorous mean-field limit results. In particular, it is possible to prove that $\rho_t^N \rightarrow \rho_t$ with a rate, as $N \rightarrow \infty$, under similar assumptions on the the finite-dimensional objective $\mathcal{E}^\#$. This justifies the study the mean-field model (4.8) to understand the convergence properties of the particle dynamics (4.2). For more details and updated references we refer to [25], and focus instead now on the convergence towards minimizers.

For $\alpha > 0$, recall the particle weights are given by $\omega(\mu) = \exp(-\alpha\mathcal{E}(\mu))$, and let us consider the corresponding finite-dimensional ones $\omega^\#(z) := \exp(-\alpha\mathcal{E}^\#(z))$ for $z \in \mathbb{R}^d \times \text{Sym}_d$. The cornerstone of the convergence analysis of CBO methods is the Laplace principle [21] which states that for a compactly supported $\rho \in \mathcal{P}(\mathbb{R}^d \times \text{Sym}_d)$, it holds

$$\lim_{\alpha \rightarrow \infty} -\frac{1}{\alpha} \log \left(\int \exp(-\alpha\mathcal{E}^\#(z)) \rho(dz) \right) = \inf_{z \in \text{supp}(\rho)} \mathcal{E}^\#(z). \quad (4.9)$$

For a quantitative version in terms of consensus points and global minimizers see [24, Proposition 4.5]. In the following, we denote with $\text{Var}(\rho)$ the variance of a probability measure ρ : $\text{Var}(\rho) = (1/2) \int \|z_1 - z_2\|^2 \rho(dz_1) \rho(dz_2)$

We recall the convergence result from [17, Assumption 3.1, Theorem 3.2] applied to the finite dimensional setting in the space $\mathbb{R}^d \times \text{Sym}_d$.

Theorem 4.1. *Assume $\underline{\mathcal{E}} := \inf \mathcal{E}^\# > -\infty$, $\mathcal{E}^\# \in \mathcal{C}^2(\mathbb{R}^d \times \text{Sym}_d)$ with bounded second derivatives, that is, for an orthonormal basis $\{e_\ell\}_{\ell=1}^D$, $D = d + d(d+1)/2$ there exists $c_{\mathcal{E}}$ such that*

$$\max_\ell \max_z \left| \frac{\partial^2 \mathcal{E}^\#(z)}{\partial e_\ell^2} \right| < c_{\mathcal{E}}. \quad (4.10)$$

If α, λ, σ and the initial distribution ρ_0 is chosen such that $\text{argmin} \mathcal{E} \subset \text{supp}(\rho_0)$ and

$$\begin{aligned} C_1 &:= 2\lambda - \sigma^2 - 2\sigma^2 \frac{e^{-\alpha\underline{\mathcal{E}}}}{\|\omega^\#\|_{L^2(\rho_0)}} > 0, \\ C_2 &:= \frac{2\text{Var}(\rho_0)}{C_1 \|\omega^\#\|_{L^2(\rho_0)}} \alpha e^{-\alpha\underline{\mathcal{E}}} c_{\mathcal{E}} (2\lambda + \sigma^2) \leq \frac{3}{4}, \end{aligned}$$

then $\text{Var}(\rho_t) \rightarrow 0$ exponentially fast and there exists \tilde{z} such that the consensus point and $\int z \rho_t(dz)$ converge to \tilde{z} exponentially fast. Moreover, it holds that

$$\mathcal{E}^\#(\tilde{z}) \leq \underline{\mathcal{E}} + r(\alpha) + \frac{\log 2}{\alpha},$$

where $r(\alpha) := -(1/\alpha) \log \|\omega^\#\|_{L^2(\rho_0)} - \underline{\mathcal{E}} \rightarrow 0$ as $\alpha \rightarrow \infty$ by the Laplace principle (4.9).

Remark 4.2. We note that parameters λ, σ, α and ρ_0 can always be picked to satisfy the Theorem's assumption by choosing, for C_1 , σ sufficiently small, and for C_2 , $\text{Var}(\rho_0)$ sufficiently small.

For \mathcal{V} and \mathcal{W} , differentiability with respect to the mean follows directly from that of V and W . Let $\mu = \mathcal{N}(m, \Sigma)$, we have (see [32, Appendix D])

$$\nabla_m \mathcal{V}(\mu) = \int \nabla V(x) \mu(dx) \quad \text{and} \quad \nabla_m^2 \mathcal{V}(\mu) = \int \nabla^2 V(x) \mu(dx).$$

With respect to the covariance,

$$\partial_{\Sigma_{ij}} \mathcal{V}(\mu) = c_{ij} \int \partial_{ij}^2 V(x) \mu(dx) \quad \text{with} \quad c_{ij} = \begin{cases} 1/2 & \text{if } i \neq j \\ 1 & \text{otherwise} \end{cases}$$

and consequently $\partial_{\Sigma_{ij}\Sigma_{\ell k}}^2 \mathcal{V}(\mu) = c_{ij}c_{\ell k} \int \partial_{ij\ell k}^4 V(x) \mu(dx)$. Hence, if $V \in \mathcal{C}^4(\mathbb{R}^d)$ with bounded second- and fourth-order derivatives, then \mathcal{V} satisfies the regularity assumptions above.

To compute the derivatives of \mathcal{W} , we view $\mu \otimes \mu$ as a Gaussian measure on $\mathbb{R}^d \times \mathbb{R}^d$ with mean (m, m) and block-diagonal covariance $\text{diag}(\Sigma, \Sigma)$, so we can re-use the computations done for \mathcal{V} variable-wise. Recall $\mathcal{W}(\mu)$ is defined in (4.5), so we have

$$\begin{aligned}\nabla_m \mathcal{W}(\mu) &= \iint (\nabla_x W(x, y) + \nabla_y W(x, y)) \mu(dx) \mu(dy), \\ \nabla_m^2 \mathcal{W}(\mu) &= \iint (\nabla_{xx}^2 W(x, y) + \nabla_{yy}^2 W(x, y) + \nabla_{xy}^2 W(x, y) + \nabla_{yx}^2 W(x, y)) \mu(dx) \mu(dy).\end{aligned}$$

With respect to the covariance, we compute

$$\partial_{\Sigma_{ij}} \mathcal{W}(\mu) = c_{ij} \iint (\partial_{x_i x_j}^2 W(x, y) + \partial_{y_i y_j}^2 W(x, y)) \mu(dx) \mu(dy),$$

with c_{ij} as before, and consequently

$$\begin{aligned}\partial_{\Sigma_{ij}\Sigma_{\ell k}}^2 \mathcal{W}(\mu) &= c_{ij}c_{\ell k} \iint \left(\partial_{x_i x_j x_{\ell} x_k}^4 W(x, y) + \partial_{y_i y_j y_{\ell} y_k}^4 W(x, y) \right. \\ &\quad \left. + \partial_{x_i x_j}^2 \partial_{y_{\ell} y_k}^2 W(x, y) + \partial_{y_i y_j}^2 \partial_{x_{\ell} x_k}^2 W(x, y) \right) \mu(dx) \mu(dy).\end{aligned}$$

Therefore, the assumptions are verified provided $W \in \mathcal{C}^4(\mathbb{R}^d \times \mathbb{R}^d)$, with bounded second- and fourth-order derivatives.

The log-entropy \mathcal{U} is invariant under mean shifts, so $\nabla_m \mathcal{U}(\mu) = 0$. For $\Sigma \in \text{Sym}_d^{++}$, see [36, Appendix A.1], it holds

$$\nabla_{\Sigma} \mathcal{U}(\mu) = -\frac{1}{2} \Sigma^{-1}.$$

Moreover, let e_{ℓ} be the ℓ -th canonical basis vector of \mathbb{R}^d , we have, see [26],

$$\frac{\partial}{\partial \Sigma_{ij}} \Sigma^{-1} = -\Sigma^{-1} e_i e_j^{\top} \Sigma^{-1}.$$

Therefore, the boundedness assumptions in Theorem 4.1 on the second derivatives, hold only on if we stay far away from singular Gaussian measures, in a subset $\Sigma \succ \varepsilon I$ for some $\varepsilon > 0$. In practice, applying a smooth eigenvalue-clipping procedure to Σ , as done in (4.7), ensures the covariance remains in this admissible set, which in turn guarantees convergence towards global minimizers. A detailed analysis of such regularization is beyond the scope of this work.

Remark 4.3. *For CBO methods, a different type of convergence result was proposed [24]. We discuss briefly the assumption considered there, and why their result is not directly applicable in our settings. The finite-dimensional objective function $\mathcal{E}^{\#}$ is not required to be differentiable but it requires to attain a unique global minimum z^* and to attain an inverse continuity assumption around z^* , see [24, Definition 3.5]. In particular, there must exists $\mathcal{E}_{\infty}, R_0, \eta > 0, \nu \in (0, \infty)$ such that*

$$\|z - z^*\|_{\text{BW}(\Sigma^0)} \leq \frac{1}{\eta} \left(\mathcal{E}^{\#}(z) - \mathcal{E}^{\#}(z^*) \right)^{\nu}$$

if $\|z\|_{\text{BW}(\Sigma^0)} \leq R_0$ and $\mathcal{E}^{\#}(z) > \mathcal{E}^{\#}(z^) + \mathcal{E}_{\infty}$ otherwise. In terms of the functional \mathcal{E} , this translates into the condition*

$$\text{LW}_{\mu^0}(\mu, \mu^*) \leq \frac{1}{\eta} (\mathcal{E}(\mu) - \mathcal{E}(\mu^*))^{\nu},$$

which is difficult to check. It is interesting to note that, for $\mathcal{E} = \text{KL}(\cdot \mid \mu^{\text{targ}})$ and if the solution coincides both with the target and the reference measure, $\mu^* = \mu^{\text{targ}} = \mu^0$, then the above condition is implied by the Talagrand's inequality [43] with constant $\lambda > 0$:

$$\mathbb{W}(\mu, \mu^{\text{targ}}) \leq \sqrt{\frac{2}{\lambda} (\text{KL}(\mu \mid \mu^{\text{targ}}) - \text{KL}(\mu^{\text{targ}} \mid \mu^{\text{targ}}))}.$$

since $\text{KL}(\mu^{\text{targ}} \mid \mu^{\text{targ}}) = 0$.

A natural question is whether Talagrand's inequality implies the growth condition in the LOT geometry in the case $\mu^* \neq \mu^{\text{targ}} \neq \mu^0$. Lower bounds of \mathbb{W} in terms of LW have been studied in [20], with further stability results in [15], showing Hölder continuity of the linearized Wasserstein distance only when μ^0 has compact support. Unfortunately, this does not apply here, as we consider Gaussian measures.

5 Numerical algorithm and experiments

In this section, we discuss the implementation aspects of the Gaussian CBO dynamics and validate its optimization capabilities against different test problems. The code used to generate the results is available at <https://github.com/borghig>.

Let $\mu^0 = \mathcal{N}(0, \Sigma^0)$, $\Sigma^0 \in \text{Sym}_d^{++}$ be a reference measure. We discretize the CBO particle dynamics (4.2) via a simple Euler–Maruyama scheme with step size $\Delta t > 0$:

$$\begin{cases} m_{(k+1)}^i &= m_{(k)}^i + \Delta t \lambda (\bar{m}^\alpha[\rho_{(k)}^N] - m_{(k)}^i) + \sqrt{\Delta t} \sigma (\bar{m}^\alpha[\rho_{(k)}^N] - m_{(k)}^i) \odot B_{(k)}^{i,m}, \\ T_{(k+1)}^i &= T_{(k)}^i + \Delta t \lambda (\bar{T}^\alpha[\rho_{(k)}^N] - T_{(k)}^i) + \sqrt{\Delta t} \sigma (\bar{T}^\alpha[\rho_{(k)}^N] - T_{(k)}^i) \odot B_{(k)}^{i,T}, \end{cases} \quad (5.1)$$

for $i = 1, \dots, N$. Here, $B_{(k)}^{i,m} \sim \mathcal{N}(0, I)$ are i.i.d., while $B_{(k)}^{i,T}$ are standard normal vectors with respect to the scalar product $\langle \cdot, \cdot \rangle_{\Sigma^0}$. We show now how to construct them.

Let $\Sigma^0 = I$ and $\{e_i\}_{i=1}^d$ be the canonical base of \mathbb{R}^d . As mentioned in Section 3.2, an orthonormal basis with respect to $\langle \cdot, \cdot \rangle_I$ is given by the matrices

$$J_{ij} = \begin{cases} e_i e_i^\top & \text{if } i = j, \\ (e_i e_j^\top + e_j e_i^\top)/\sqrt{2} & \text{if } i < j. \end{cases}$$

A standard normal vector $B \in \text{Sym}$ according to this basis can be conveniently generated as

$$B = \frac{\Xi + \Xi^\top}{2} \quad \text{with} \quad \Xi_{ij} \sim \mathcal{N}(0, 1).$$

An orthonormal basis for $\Sigma^0 = I$ can be translated into an orthonormal basis for an arbitrary $\Sigma^0 \in \text{Sym}_d^{++}$. Let $\Sigma^0 = Q \Lambda Q^\top$ be its singular value decomposition with $\Lambda = \text{diag}(\lambda_1, \dots, \lambda_d)$. An orthonormal basis for $\langle \cdot, \cdot \rangle_{\Sigma^0}$ is given by

$$\tilde{J}_{ij} = \begin{cases} \frac{1}{\sqrt{\lambda_i}} Q J_{ii} Q^\top & \text{if } i = j, \\ \frac{1}{\sqrt{\lambda_i + \lambda_j}} Q J_{ij} Q^\top & \text{if } i < j. \end{cases}$$

This can be checked by directly computing $\langle \tilde{J}_{ij}, \tilde{J}_{k\ell} \rangle_{\Sigma^0} = \text{tr}(\tilde{J}_{ij} \Sigma^0 \tilde{J}_{k\ell})$. Analogously, a standard normal vector \tilde{B} according to this basis can be constructed from a standard normal vector B for the basis $\{J_{ij}\}_{i \leq j}$ by rescaling each entry:

$$\tilde{B}_{ij} = \begin{cases} \frac{1}{\sqrt{\lambda_i}} B_{ii} & \text{if } i = j, \\ \frac{1}{\sqrt{\lambda_i + \lambda_j}} B_{ij} & \text{if } i < j, \end{cases} \quad \text{and set } \tilde{B}_{ji} = \tilde{B}_{ij}.$$

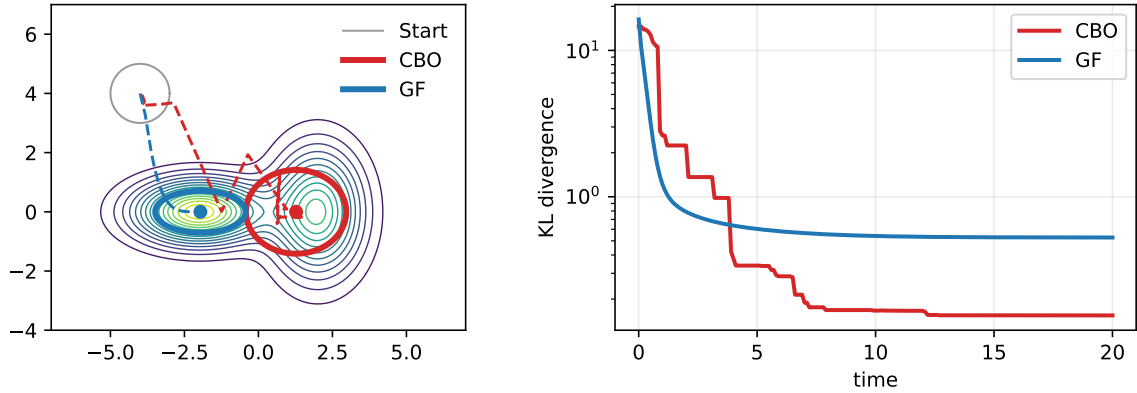


Figure 4: Comparison between one run of the CBO and GF algorithms in approximating a bimodal target density (contour lines). For CBO, the final Gaussian consensus point is shown. Trajectories of the mean of the consensus point and of the GF dynamics are also included. On the right, the evolution of the objective $\mathcal{E} = \text{KL}$ shows that CBO finds a better solution to the VI problem. Parameters: $\Delta t = 0.1, \lambda = 1, \sigma = 5, N = 20, \alpha = 10^4$. Reference measure for LBW geometry: $\mathcal{N}(0, I)$.

In our experiments, the objective is the KL divergence from the target measure $\mu^{\text{targ}} \propto \exp(-V)$, namely $\mathcal{E} = \text{KL}(\cdot | \mu^{\text{targ}})$. Recall that, to compute the consensus point $(\bar{m}^\alpha[\rho_{(k)}^N], \bar{T}^\alpha[\rho_{(k)}^N])$, we need to evaluate the functional \mathcal{E} at the particle locations. Since $\text{KL}(\mu | \mu^{\text{targ}}) = \mathcal{U}(\mu) + \mathcal{V}(\mu)$, we set $\mathcal{E}(\mu) = M = 10^4$ whenever the particle's covariance matrix is singular (when $\mathcal{U}(\mu) = +\infty$). The expected value $\mathcal{V} = \int V(x)\mu(dx)$, $V := -\log(\mu^{\text{targ}})$ is approximated using a quadrature rule based on $2d + 1$ points [4], although a Monte Carlo estimate could also be applied in high-dimensional problems.

We compare the results with the Bures–Wasserstein Gradient Flow (GF) of $\text{KL}(\mu | \mu^{\text{targ}})$ studied in [36], discretized via an explicit Euler scheme with same step size Δt and same quadrature approximation for expected values.

5.1 Tests in $d = 2$

We test the algorithm for different Gaussian Variational Inference (VI) problems where targets are Gaussian mixture models with $K = 2$ or $K = 4$ components

$$\mu^{\text{targ}} = \sum_{k=1}^K w_k \mathcal{N}(m_k, \Sigma_k) \quad (5.2)$$

see Table 1 for the exact definitions.

Since system (5.1) is over-parameterized, in CBO algorithms one typically fixes $\lambda = 1$ (see, for instance, [17]). The other parameters are set to $\Delta t = 0.1, \sigma = 5, \alpha = 10^4$, and $N = 20$. We keep $\Sigma^0 = I$ to be the reference measure throughout the computation. Given an initialization $(m_{(0)}, \Sigma_{(0)})$ for the GF algorithm, the CBO particles are initialized as $m_{(0)}^i = m_{(0)} + 0.1\xi^i, \xi^i \sim \mathcal{N}(0, I)$, and $T_{(0)}^i = \log_I(\Sigma_{(0)}) + 0.1\Xi^i$, where $\Xi_{\ell k}^i \sim \mathcal{N}(0, 1)$ and $\Xi^i = (\Xi^i)^\top$. This makes the comparison between GF and CBO fairer, as it prevents the CBO particles from exploring the search space even before the dynamics begins.

Figure 4 shows the solutions computed by CBO and GF for a test instance where the target measure is bimodal (and hence not log-concave). The trajectory of the mean of the consensus point is plotted, as well as the final computed Gaussian, represented by an ellipse. Unlike GF, the CBO trajectory follows a stochastic path, with the consensus point

Target	K	means	covariances	weights
A	2	$m_1 = (-2.2, 0.0)$ $m_2 = (2.2, 0.0)$	$\Sigma_1 = \begin{pmatrix} 1 & 0.2 \\ 0.2 & 0.6 \end{pmatrix}$ $\Sigma_2 = \begin{pmatrix} 1 & -0.2 \\ -0.2 & 0.6 \end{pmatrix}$	$w_1 = 0.5$ $w_2 = 0.5$
B	2	$m_1 = (-1.77, 1.06)$ $m_2 = (-0.35, -0.35)$	$\Sigma_1 = \begin{pmatrix} 1.25 & -0.25 \\ -0.25 & 1.25 \end{pmatrix}$ $\Sigma_2 = \begin{pmatrix} 2.50 & -1.50 \\ -1.50 & 2.50 \end{pmatrix}$	$w_1 = 0.5$ $w_2 = 0.5$
C	4	$m_1 = (-2.47, 1.06)$ $m_2 = (-1.48, 0.64)$ $m_3 = (-2.05, 0.07)$ $m_4 = (0.20, -1.61)$	$\Sigma_1 = \begin{pmatrix} 0.45 & 0 \\ 0 & 0.45 \end{pmatrix}$ $\Sigma_2 = \begin{pmatrix} 1.9 & -1.9 \\ -1.9 & 2.3 \end{pmatrix}$ $\Sigma_3 = \begin{pmatrix} 2.3 & -1.9 \\ -1.9 & 1.9 \end{pmatrix}$ $\Sigma_4 = \begin{pmatrix} 2.51 & -2.49 \\ -2.49 & 2.51 \end{pmatrix}$	$w_1 = 0.25$ $w_2 = 0.30$ $w_3 = 0.30$ $w_4 = 0.15$
D	4	$m_1 = (-1.5, -2.0)$ $m_2 = (1.5, 0.7)$ $m_3 = (-1.5, 0.7)$ $m_4 = (1.5, -2.0)$	$\Sigma_1 = \Sigma_2 = \Sigma_3 = \Sigma_4 = \begin{pmatrix} 0.7 & 0 \\ 0 & 0.5 \end{pmatrix}$	$w_1 = 0.2$ $w_2 = 0.2$ $w_3 = 0.2$ $w_4 = 0.4$

Table 1: Gaussian mixture model parameters (means, covariances, and mixture weights) for targets A–D, see (5.2).

exploring the search space before converging to its final location. This leads to a slower initial decay of the KL divergence, but CBO ultimately finds a better solution than GF, which becomes trapped in a sub-optimal mode.

We perform the same experiments for different target measures (A, B, C, and D) and collect statistics over 100 runs. The starting points $(m_{(0)}, \Sigma_{(0)})$ are initialized as $m_{(0)} \sim \text{Unif}([-5, 5]^2)$ and $\Sigma_{(0)} = I$ in all runs for both CBO and GF. For all targets, Figure 5 shows one illustrative run and the median KL divergence over time, together with the $[0.25, 0.75]$ interquartile range. CBO outperforms GF in all scenarios considered: not only for non-logconcave targets (Figures 5A, 5D) but also for unimodal ones (Figures 5B, 5C). For test case C, the time step is reduced to $\Delta t = 0.05$ to avoid numerical instability in the GF discretization.

In CBO algorithms, the diffusion parameter σ is crucial for balancing particle exploration of the search space with the emergence of consensus. Small values of σ may lead to premature convergence, while large values can prevent convergence altogether. Values $\sigma \in [3, 5]$ yield the best performance across all test problems considered (see Figure 6A).

The number of particles N is also an important choice, as it determines the trade-off between computational accuracy and efficiency. In the tests considered, however, there is little improvement beyond $N = 16$ particles, as shown in Figure 6B.

We also test the impact on the linearization procedure. So far we have kept the base measure for the LBW geometry to be the standard normal distribution $\mathcal{N}(0, I)$, that is, $\Sigma^0 = I$. To mitigate the (eventual) loss in geometry information, it is natural to think of updating the reference measure during the computation, from time to time, to linearize the space around the current consensus point. We tested this strategy for different update frequencies $\Delta t_{\text{up}} > 0$, from the smallest one possible, $\Delta t_{\text{up}} = \Delta t = 0.1$ to no update at all $\Delta t_{\text{up}} = 12.8 > T_{\text{max}} = 10$. As we can notice from the results of the experiments, see Figure 6C, in the problem considered there is no benefit in updating the base measure. For the target measure C, the update strategy actually deteriorates the algorithm's accuracy. We conjecture this may be due to the numerical error introduced by frequently computing the logarithmic and exponential BW maps.

5.2 Tests in $d = 10$

We evaluate GF and CBO on synthetic Gaussian mixtures in dimension $d = 10$. Each target distribution is a randomly generated K -component Gaussian mixture model:

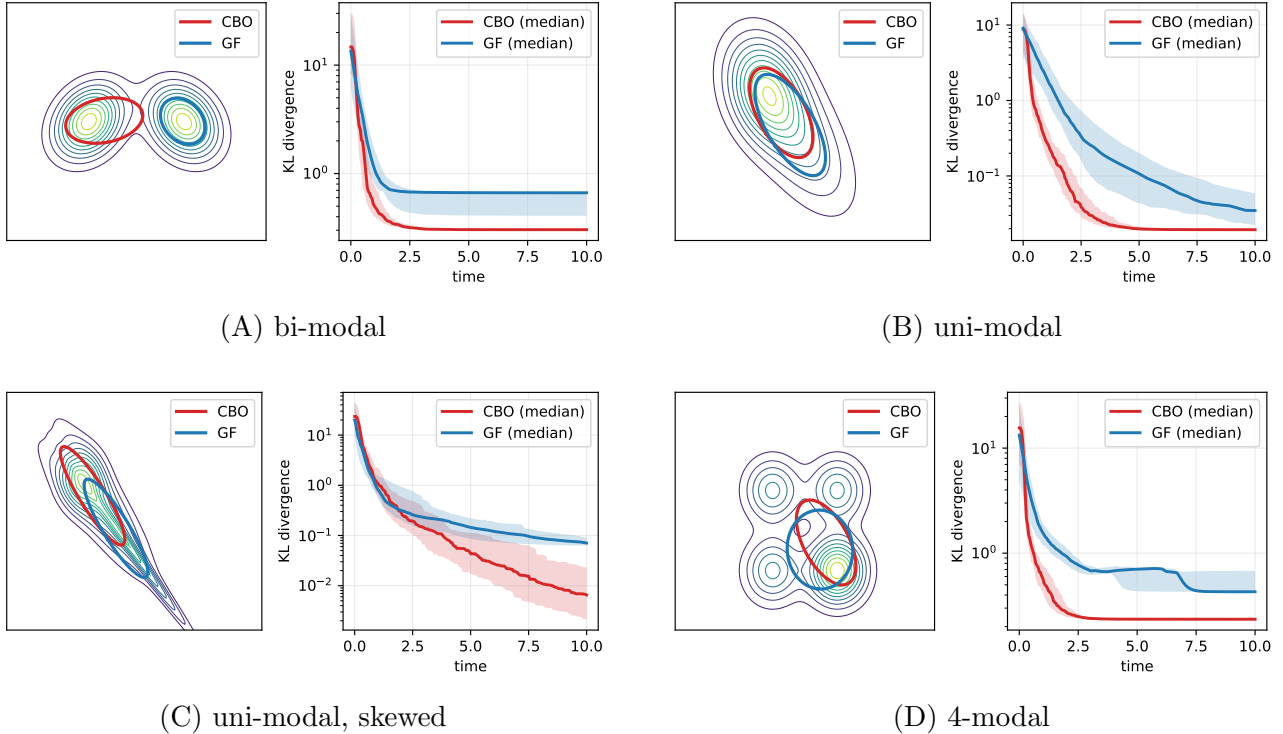


Figure 5: Comparison between CBO and GF algorithms in approximating different target densities given by Gaussian mixture models with 2 components (A, B) and 4 components (C, D) (see Table 1). The 2D plots show the computed solutions for a single run, while the KL evolution is averaged over 100 runs with different random initializations. Median and [0.25, 0.75] interquartile ranges are shown. Parameters: $\Delta t = 0.1$ (except for C, where $\Delta t = 0.05$), $\lambda = 1, \sigma = 5, N = 20, \alpha = 10^4$. Reference measure for LBW geometry: $\mathcal{N}(0, I)$. Supplementary videos illustrating the evolution of the GF and CBO algorithms are available here [9].

mixture weights are sampled from a Dirichlet distribution, component means are sampled uniformly on the sphere of radius $R_{\text{mean}}\sqrt{d}$ (so that components are well separated in high dimension, with R_{mean} controlling the spread), and component covariances are random SPD matrices with eigenvalues in $[\lambda_{\min}, \lambda_{\max}]$.

We set $d = 10, K = 5, R_{\text{mean}} = 3.0, \lambda_{\min} = 0.4$, and $\lambda_{\max} = 2.0$. Both methods are initialized from a Gaussian centered at a random point near the origin with covariance equal to the identity, and we run them for a horizon $T = 75$ with step size $\Delta t = 0.1$. For CBO we employ $N = 100$ particles with parameters $\alpha = 10^4, \sigma = 2.5, \lambda = 1.0$, and we do not update the base.

To compare methods robustly, we generate $M = 20$ independent random GMM instances and record the evolution of $\text{KL}(\mu \mid \mu^{\text{targ}})$ for each method. Since absolute KL values vary between instances, each trajectory is normalized by the best KL value achieved on that instance,

$$\text{RelKL}_i(t) = \frac{\text{KL}_i(t)}{K_i^*}, \quad K_i^* = \min_{t,m} \text{KL}_i^m(t),$$

where i indexes the instance and $m \in \{\text{CBO}, \text{GF}\}$ the method. We then report the relative KL, $\text{RelKL}_i(t)$, aggregated across instances by plotting the median together with the interquartile range [0.25, 0.75].

From Figure 7, we notice that the interquartile range of CBO is smaller than that of GF. We conjecture that GF may sometimes get stuck in local minima, while CBO computes more robust solutions across different instances of the problem thanks to the

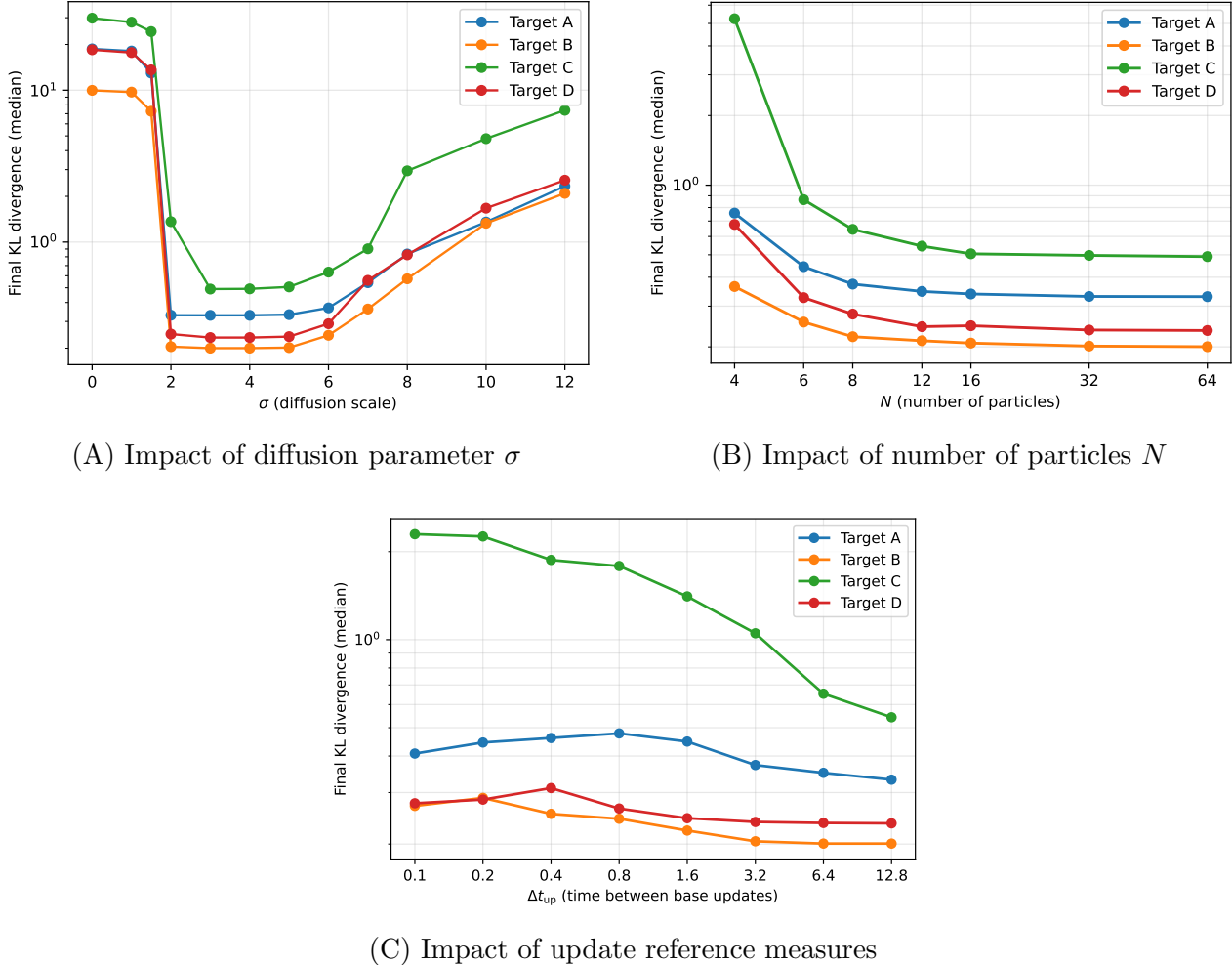


Figure 6: Sensitivity analysis of CBO performance with respect to (A) the diffusion parameter σ , (B) the number of particles N , (C) update frequency of the reference measure $\mu_0 = \mathcal{N}(0, \Sigma^0)$. The curves show the median KL divergence averaged across 100 runs with different random initializations. Same parameters as experiment in Figure 5.

particle exploration. On average, the Gaussian CBO algorithm computes better solutions than GF for this class of problems.

Remark 5.1. *We note that extensions of particle-based optimizers to very high dimensions typically require additional heuristics to keep the computational cost manageable. For instance, in [17] a random batch technique for the computation of the consensus point was proposed to reduce the number of function evaluations per step. Another delicate aspect is the choice of the diffusion parameter σ . As noted in [10, Section 4.3], the interval of values of σ leading to good performance tends to shrink as d increases, and particles become more prone either to converge prematurely or to diverge. To tackle high-dimensional machine learning problems, in [17] the authors also propose a heuristic in which a relatively small σ is used, but particles are re-initialized with white noise at the end of each training epoch. Such strategies may also be applied in our context to address high-dimensional Gaussian VI problems.*

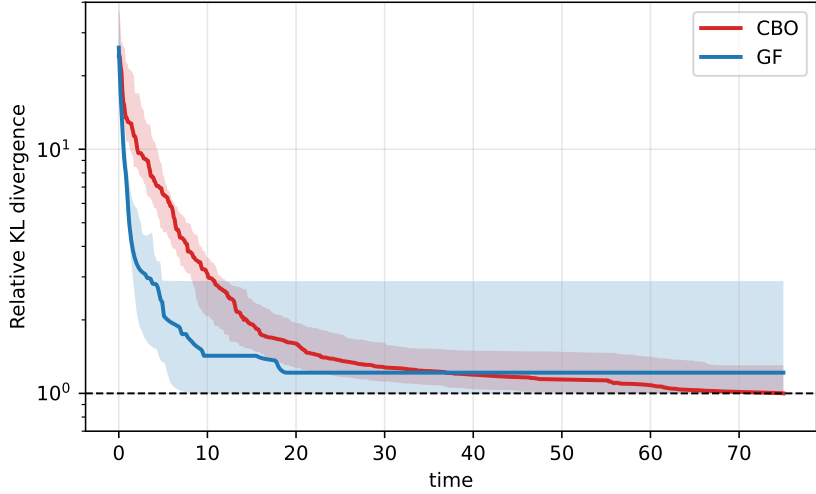


Figure 7: Comparison between CBO and GF in approximating Gaussian mixture targets ($K = 5$) in $d = 10$. The curves report the relative KL divergence $\text{RelKL}(t) = \text{KL}(t)/K^*$, normalized by the best value achieved on each instance, and averaged across $M = 20$ random mixtures. Median and $[0.25, 0.75]$ interquartile ranges are shown. Parameters: $\Delta t = 0.1$, $T = 75$, $\lambda = 1$, $\sigma = 2.5$, $N = 100$, $\alpha = 10^4$. Base measure not updated.

6 Outlook

In this work, we have introduced a new computational paradigm based on Gaussian particles evolving according to a stochastic CBO-type dynamics in the Linearized Bures–Wasserstein (LBW) space. The proposed framework enables efficient simulation of interacting particle systems while preserving essential features of the underlying Bures–Wasserstein geometry. Beyond the specific algorithm developed here, the LBW representation opens the door to a variety of new optimization dynamics on the space of Gaussian measures.

Our stochastic analysis in LBW is not limited to CBO. The same ideas could be applied to enhance the robustness of existing Gaussian variational inference methods—such as Gradient Flows (GF)—against local minima, by injecting geometrically consistent noise. In particular, we are currently investigating the formulation and analysis of Stochastic Gradient Flows (SGF) in LBW space.

It is also natural to ask whether one can define and simulate the particle dynamics directly in the full Bures–Wasserstein space, without relying on linearization. This would require a careful and computationally efficient treatment of singular Gaussians, which is nontrivial in the non-linear geometry of \mathcal{N}^d .

Finally, the optimal transport perspective naturally suggests extensions beyond the Gaussian setting via Linear Optimal Transport (LOT) [14, 35, 40, 52]. Our method can be seen as a CBO-type dynamics on affine maps $\mathcal{T}^i(x) = m^i + (I + T^i)x$ with $m^i \in \mathbb{R}^d$ and $T^i \in \text{Sym}$, which induce Gaussian agents via $\mu^i = \mathcal{T}_\#^i \mu^0$. This can be extended by replacing affine maps with general square-integrable maps $\mathcal{T}^i \in L^2(\mu^0; \mathbb{R}^d)$, thereby evolving arbitrary probability measures $\mu^i = \mathcal{T}_\#^i \mu^0$ in $\mathcal{P}_2(\mathbb{R}^d)$ within the same CBO-type framework.

Acknowledgment

GB was supported by the Wolfson Fellowship of the Royal Society “Uncertainty quantification, data-driven simulations and learning of multiscale complex systems governed

by PDEs” of Prof. L. Pareschi at Heriot-Watt University. JAC was supported by the Advanced Grant Nonlocal-CPD (Nonlocal PDEs for Complex Particle dynamics: Phase Transitions, Patterns and Synchronization) of the European Research Council Executive Agency (ERC) under the European Union’s Horizon 2020 research and innovation programme (grant agreement No. 883363). JAC was also partially supported by the “Maria de Maeztu” Excellence Unit IMAG, reference CEX2020-001105-M, funded by the Spanish ministry of Science MCIN/AEI/10.13039/501100011033/ and the EPSRC grant numbers EP/T022132/1 and EP/V051121/1.

References

- [1] M. Aguech and G. Carlier. Barycenters in the Wasserstein space. *SIAM Journal on Mathematical Analysis*, 43(2):904–924, 2011. [arXiv:https://doi.org/10.1137/100805741](https://arxiv.org/abs/https://doi.org/10.1137/100805741), [doi:10.1137/100805741](https://doi.org/10.1137/100805741).
- [2] D. Alvarez-Melis, Y. Schiff, and Y. Mroueh. Optimizing functionals on the space of probabilities with input convex neural networks. *Transactions on Machine Learning Research*, 2022. URL: <https://openreview.net/forum?id=dp0YN7o8Jm>.
- [3] L. Ambrosio, N. Gigli, and G. Savaré. *Gradient Flows in Metric Spaces and in the Space of Probability Measures*. Lectures in Mathematics ETH Zürich. Birkhäuser, 2. ed edition, 2008. OCLC: 254181287.
- [4] I. Arasaratnam and S. Haykin. Cubature Kalman filters. *IEEE Transactions on Automatic Control*, 54(6):1254–1269, 2009. [doi:10.1109/TAC.2009.2019800](https://doi.org/10.1109/TAC.2009.2019800).
- [5] R. Bhatia, T. Jain, and Y. Lim. On the Bures–Wasserstein distance between positive definite matrices. *Expositiones Mathematicae*, 37(2):165–191, 2019. URL: <https://www.sciencedirect.com/science/article/pii/S0723086918300021>, [doi:10.1016/j.exmath.2018.01.002](https://doi.org/10.1016/j.exmath.2018.01.002).
- [6] A. N. Bishop and A. Doucet. Distributed nonlinear consensus in the space of probability measures. *IFAC Proceedings Volumes*, 47(3):8662–8668, 2014. 19th IFAC World Congress. URL: <https://www.sciencedirect.com/science/article/pii/S1474667016429800>, [doi:10.3182/20140824-6-ZA-1003.00341](https://doi.org/10.3182/20140824-6-ZA-1003.00341).
- [7] A. N. Bishop and A. Doucet. Network consensus in the Wasserstein metric space of probability measures. *SIAM Journal on Control and Optimization*, 59(5):3261–3277, 2021. [arXiv:https://doi.org/10.1137/19M1268252](https://arxiv.org/abs/https://doi.org/10.1137/19M1268252), [doi:10.1137/19M1268252](https://doi.org/10.1137/19M1268252).
- [8] D. M. Blei, A. Kucukelbir, and J. D. McAuliffe. Variational inference: A review for statisticians. *Journal of the American Statistical Association*, 112(518):859–877, 2017. [arXiv:https://doi.org/10.1080/01621459.2017.1285773](https://arxiv.org/abs/https://doi.org/10.1080/01621459.2017.1285773), [doi:10.1080/01621459.2017.1285773](https://doi.org/10.1080/01621459.2017.1285773).
- [9] G. Borghi and J. Carrillo. Variational inference via Gaussian interacting particles in the Bures–Wasserstein geometry, 2025. Media. [doi:10.6084/m9.figshare.30958322](https://doi.org/10.6084/m9.figshare.30958322).
- [10] G. Borghi, M. Herty, and L. Pareschi. Constrained consensus-based optimization. *SIAM Journal on Optimization*, 33(1):211–236, 2023. [arXiv:https://doi.org/10.1137/22M1471304](https://arxiv.org/abs/https://doi.org/10.1137/22M1471304), [doi:10.1137/22M1471304](https://doi.org/10.1137/22M1471304).
- [11] G. Borghi, M. Herty, and L. Pareschi. Kinetic models for optimization: A unified mathematical framework for metaheuristics. *arXiv preprint arXiv:2410.10369*, 2024. URL: <https://arxiv.org/abs/2410.10369>, [arXiv:2410.10369](https://arxiv.org/abs/2410.10369).
- [12] G. Borghi, M. Herty, and A. Stavitskiy. Dynamics of measure-valued agents in the space of probabilities. *SIAM Journal on Mathematical Analysis*, 57(5):5107–5134, 2025. [arXiv:https://doi.org/10.1137/24M1675515](https://arxiv.org/abs/https://doi.org/10.1137/24M1675515), [doi:10.1137/24M1675515](https://doi.org/10.1137/24M1675515).

- [13] Y. Brenier. Polar factorization and monotone rearrangement of vector-valued functions. *Communications on Pure and Applied Mathematics*, 44(4):375–417, 1991. URL: <https://onlinelibrary.wiley.com/doi/abs/10.1002/cpa.3160440402>, arXiv: <https://onlinelibrary.wiley.com/doi/pdf/10.1002/cpa.3160440402>, doi:10.1002/cpa.3160440402.
- [14] T. Cai, J. Cheng, N. Craig, and K. Craig. Linearized optimal transport for collider events. *Phys. Rev. D*, 102:116019, Dec 2020. URL: <https://link.aps.org/doi/10.1103/PhysRevD.102.116019>, doi:10.1103/PhysRevD.102.116019.
- [15] G. Carlier, A. Delalande, and Q. Mérigot. Quantitative stability of the pushforward operation by an optimal transport map. *Foundations of Computational Mathematics*, 2024. doi:10.1007/s10208-024-09669-4.
- [16] J. A. Carrillo, Y.-P. Choi, C. Totzeck, and O. Tse. An analytical framework for consensus-based global optimization method. *Math. Models Methods Appl. Sci.*, 28(6):1037–1066, 2018. doi:10.1142/S0218202518500276.
- [17] J. A. Carrillo, S. Jin, L. Li, and Y. Zhu. A consensus-based global optimization method for high dimensional machine learning problems. *ESAIM: Control, Optimisation and Calculus of Variations*, 27:S5, 2021.
- [18] S. Chewi, T. Maunu, P. Rigollet, and A. Stromme. Gradient descent algorithms for Bures-Wasserstein barycenters. In J. Abernethy and S. Agarwal, editors, *Proceedings of Thirty Third Conference on Learning Theory*, volume 125 of *Proceedings of Machine Learning Research*, pages 1276–1304. PMLR, 09–12 Jul 2020. URL: <https://proceedings.mlr.press/v125/chewi20a.html>.
- [19] P. Cisneros-Velarde and F. Bullo. Distributed Wasserstein barycenters via displacement interpolation. *IEEE Transactions on Control of Network Systems*, 10(2):785–795, 2023. doi:10.1109/TCNS.2022.3210341.
- [20] A. Delalande and Q. Merigot. Quantitative stability of optimal transport maps under variations of the target measure. *Duke Mathematical Journal*, 172(17):3321–3357, 2023.
- [21] A. Dembo and O. Zeitouni. *Large Deviations Techniques and Applications*. Springer-Verlag Berlin Heidelberg, 2010.
- [22] M. Z. Diao, K. Balasubramanian, S. Chewi, and A. Salim. Forward-backward Gaussian variational inference via JKO in the Bures-Wasserstein space. In A. Krause, E. Brunskill, K. Cho, B. Engelhardt, S. Sabato, and J. Scarlett, editors, *Proceedings of the 40th International Conference on Machine Learning*, volume 202 of *Proceedings of Machine Learning Research*, pages 7960–7991. PMLR, 23–29 Jul 2023. URL: <https://proceedings.mlr.press/v202/diao23a.html>.
- [23] D. Dowson and B. Landau. The Fréchet distance between multivariate normal distributions. *Journal of Multivariate Analysis*, 12(3):450–455, 1982. URL: <https://www.sciencedirect.com/science/article/pii/0047259X8290077X>, doi:10.1016/0047-259X(82)90077-X.
- [24] M. Fornasier, T. Klock, and K. Riedl. Consensus-based optimization methods converge globally. *SIAM Journal on Optimization*, 34(3):2973–3004, 2024. arXiv:<https://doi.org/10.1137/22M1527805>, doi:10.1137/22M1527805.
- [25] N. Gerber, F. Hoffmann, D. Kim, and U. Vaes. Uniform-in-time propagation of chaos for consensus-based optimization. *arXiv preprint arXiv:2505.08669*, 2025.
- [26] M. B. Giles. Collected matrix derivative results for forward and reverse mode algorithmic differentiation. In C. H. Bischof, H. M. Bücker, P. Hovland, U. Naumann,

and J. Utke, editors, *Advances in Automatic Differentiation*, pages 35–44, Berlin, Heidelberg, 2008. Springer Berlin Heidelberg.

[27] C. R. Givens and R. M. Shortt. A class of Wasserstein metrics for probability distributions. *Michigan Mathematical Journal*, 31(2):231–240, 1984.

[28] A. Han, B. Mishra, P. Jawanpuria, and J. Gao. On Riemannian optimization over positive definite matrices with the Bures–Wasserstein geometry. In A. Beygelzimer, Y. Dauphin, P. Liang, and J. W. Vaughan, editors, *Advances in Neural Information Processing Systems*, 2021. URL: <https://openreview.net/forum?id=ZCHxGFmc62a>.

[29] J. Holland. *Adaptation in Natural and Artificial Systems: An Introductory Analysis with Applications to Biology, Control, and Artificial Intelligence*. University of Michigan Press, 1975. URL: <https://books.google.co.uk/books?id=JE5RAAAAMAAJ>.

[30] A. Katsevich and P. Rigollet. On the approximation accuracy of Gaussian variational inference. *The Annals of Statistics*, 52(4):1384–1409, 2024. [doi:10.1214/24-AOS2393](https://doi.org/10.1214/24-AOS2393).

[31] J. Kennedy and R. Eberhart. Particle swarm optimization. In *Proceedings of ICNN’95-international conference on neural networks*, volume 4, pages 1942–1948. ieee, 1995.

[32] M. E. Khan and H. Rue. The Bayesian learning rule. *J. Mach. Learn. Res.*, 24(1), Jan. 2023.

[33] S. Kirkpatrick, C. D. Gelatt, and M. P. Vecchi. Optimization by simulated annealing. *Science*, 220(4598):671–680, 1983. URL: <https://www.science.org/doi/abs/10.1126/science.220.4598.671>, arXiv:<https://www.science.org/doi/pdf/10.1126/science.220.4598.671>, doi:[10.1126/science.220.4598.671](https://doi.org/10.1126/science.220.4598.671).

[34] J. Knoblauch, J. Jewson, and T. Damoulas. An optimization-centric view on Bayes’ rule: Reviewing and generalizing variational inference. *Journal of Machine Learning Research*, 23(132):1–109, 2022. URL: <http://jmlr.org/papers/v23/19-1047.html>.

[35] S. Kolouri, A. B. Tosun, J. A. Ozolek, and G. K. Rohde. A continuous linear optimal-transport approach for pattern analysis in image datasets. *Pattern recognition*, 51:453–462, 2016.

[36] M. Lambert, S. Chewi, F. Bach, S. Bonnabel, and P. Rigollet. Variational inference via Wasserstein gradient flows. In A. H. Oh, A. Agarwal, D. Belgrave, and K. Cho, editors, *Advances in Neural Information Processing Systems*, 2022. URL: <https://openreview.net/forum?id=K2PTuvVTF1L>.

[37] M. Liero, A. Mielke, O. Tse, and J.-J. Zhu. Evolution of Gaussians in the Hellinger-Kantorovich-Boltzmann gradient flow. *Communications on Pure and Applied Analysis*, (early access), 2025. URL: <https://www.aimscolleges.org/article/id/68ecc16acb5dde21e7544b1b>, doi:[10.3934/cpaa.2025105](https://doi.org/10.3934/cpaa.2025105).

[38] J. Lott. Some geometric calculations on Wasserstein space. *Communications in Mathematical Physics*, 277(2):423–437, 2008. [doi:10.1007/s00220-007-0367-3](https://doi.org/10.1007/s00220-007-0367-3).

[39] L. Malagò, L. Montrucchio, and G. Pistone. Wasserstein Riemannian geometry of Gaussian densities. *Information Geometry*, 1(2):137–179, Dec 2018. [doi:10.1007/s41884-018-0014-4](https://doi.org/10.1007/s41884-018-0014-4).

[40] C. Moosmüller and A. Cloninger. Linear optimal transport embedding: provable Wasserstein classification for certain rigid transformations and perturbations. *Information and Inference: A Journal of the IMA*, 12(1):363–389, 2023.

[41] I. Olkin and F. Pukelsheim. The distance between two random vectors with given dispersion matrices. *Linear Algebra and its Applications*, 48:257–263, 1982. URL: <https://www.sciencedirect.com/science/article/pii/0024379582901124>, doi:[10.1016/0024-3795\(82\)90112-4](https://doi.org/10.1016/0024-3795(82)90112-4).

[42] F. Otto. The geometry of dissipative evolution equations: The porous medium equation. *Communications in Partial Differential Equations*, 26(1-2):101–174, 2001. [doi:10.1081/PDE-100002243](https://doi.org/10.1081/PDE-100002243).

[43] F. Otto and C. Villani. Generalization of an inequality by Talagrand and links with the logarithmic Sobolev inequality. *Journal of Functional Analysis*, 173(2):361–400, 2000. URL: <https://www.sciencedirect.com/science/article/pii/S0022123699935577>, [doi:10.1006/jfan.1999.3557](https://doi.org/10.1006/jfan.1999.3557).

[44] X. Pennec, P. Fillard, and N. Ayache. A Riemannian framework for tensor computing. *International Journal of Computer Vision*, 66(1):41–66, 2006. [doi:10.1007/s11263-005-3222-z](https://doi.org/10.1007/s11263-005-3222-z).

[45] R. Pettersson. Projection scheme for stochastic differential equations with convex constraints. *Stochastic Processes and their Applications*, 88(1):125–134, 2000. URL: <https://www.sciencedirect.com/science/article/pii/S0304414999001210>, [doi:10.1016/S0304-4149\(99\)00121-0](https://doi.org/10.1016/S0304-4149(99)00121-0).

[46] A. Pilipenko. *An introduction to stochastic differential equations with reflection*. Universitätsverlag Potsdam, 2014.

[47] R. Pinna, C. Totzeck, O. Tse, and S. Martin. A consensus-based model for global optimization and its mean-field limit. *Math. Models Methods Appl. Sci.*, 27(1):183–204, 2017. [doi:10.1142/S0218202517400061](https://doi.org/10.1142/S0218202517400061).

[48] Y. Polyanskiy and Y. Wu. Wasserstein continuity of entropy and outer bounds for interference channels. *IEEE Transactions on Information Theory*, 62(7):3992–4002, 2016.

[49] P. Ren and F.-Y. Wang. Ornstein–Uhlenbeck type processes on Wasserstein spaces. *Stochastic Processes and their Applications*, 172:104339, 2024. [doi:10.1016/j.spa.2024.104339](https://doi.org/10.1016/j.spa.2024.104339).

[50] L. Rüschendorf and L. Uckelmann. On the n-coupling problem. *Journal of Multivariate Analysis*, 81(2):242–258, 2002. URL: <https://www.sciencedirect.com/science/article/pii/S0047259X01920056>, [doi:10.1006/jmva.2001.2005](https://doi.org/10.1006/jmva.2001.2005).

[51] F. Santambrogio. *Optimal Transport for Applied Mathematicians*. Birkhäuser, 2015.

[52] C. Sarrazin and B. Schmitzer. Linearized optimal transport on manifolds. *SIAM Journal on Mathematical Analysis*, 56(4):4970–5016, 2024. [arXiv:https://doi.org/10.1137/23M1564535](https://arxiv.org/abs/23M1564535), [doi:10.1137/23M1564535](https://doi.org/10.1137/23M1564535).

[53] V. Simoncini. Computational methods for linear matrix equations. *SIAM Review*, 58(3):377–441, 2016. [arXiv:https://doi.org/10.1137/130912839](https://arxiv.org/abs/130912839), [doi:10.1137/130912839](https://doi.org/10.1137/130912839).

[54] V. Spokoiny and M. Panov. Accuracy of Gaussian approximation for high-dimensional posterior distributions. *Bernoulli*, 31(2):843 – 867, 2025. [doi:10.3150/21-BEJ1412](https://doi.org/10.3150/21-BEJ1412).

[55] A.-S. Sznitman. Topics in propagation of chaos. In *Ecole d’été de probabilités de Saint-Flour XIX—1989*, pages 165–251. Springer, 1991.

[56] A. Takatsu. Wasserstein geometry of Gaussian measures. *Osaka Journal of Mathematics*, 48(4):1005 – 1026, 2011.

[57] Y. Thanwerdas and X. Pennec. Bures–Wasserstein minimizing geodesics between covariance matrices of different ranks. *SIAM Journal on Matrix Analysis and Applications*, 44(3):1447–1476, 2023. [arXiv:https://doi.org/10.1137/22M149168X](https://arxiv.org/abs/22M149168X), [doi:10.1137/22M149168X](https://doi.org/10.1137/22M149168X).

- [58] L. Tierney and J. B. Kadane. Accurate approximations for posterior moments and marginal densities. *Journal of the American Statistical Association*, 81(393):82–86, 1986. URL: <https://www.tandfonline.com/doi/abs/10.1080/01621459.1986.10478240>, arXiv:<https://www.tandfonline.com/doi/pdf/10.1080/01621459.1986.10478240>, doi:10.1080/01621459.1986.10478240.
- [59] A. Uhlmann. The metric of Bures and the geometric phase. *Quantum groups and related topics*, pages 267–264, 1992.
- [60] T. Vayer and R. Gribonval. Controlling Wasserstein distances by kernel norms with application to compressive statistical learning. *Journal of Machine Learning Research*, 24(149):1–51, 2023. URL: <http://jmlr.org/papers/v24/21-1516.html>.
- [61] Y. Zemel and V. M. Panaretos. Fréchet means and Procrustes analysis in Wasserstein space. *Bernoulli*, 25(2):932 – 976, 2019. doi:10.3150/17-BEJ1009.
- [62] P. C. Álvarez Esteban, E. del Barrio, J. Cuesta-Albertos, and C. Matrán. A fixed-point approach to barycenters in Wasserstein space. *Journal of Mathematical Analysis and Applications*, 441(2):744–762, 2016. URL: <https://www.sciencedirect.com/science/article/pii/S0022247X16300907>, doi:10.1016/j.jmaa.2016.04.045.